

# Potential Energy Surface and Product Branching Ratios for the Reaction of Dicarbon, $C_2(X^1\Sigma_g^+)$ , with Methylacetylene, $CH_3CCH(X^1A_1)$ : An Ab Initio/RRKM Study

A. M. Mebel,<sup>\*,†</sup> V. V. Kislov, and R. I. Kaiser<sup>‡</sup>

Department of Chemistry and Biochemistry, Florida International University, Miami, Florida 33199, and Department of Chemistry, University of Hawaii at Manoa, Honolulu, Hawaii 96822-2275

Received: August 3, 2005; In Final Form: November 4, 2005

Ab initio calculations of the potential energy surface for the  $C_2(X^1\Sigma_g^+) + CH_3CCH(X^1A_1)$  reaction have been carried at the G2M level of theory. The calculations show that the dicarbon molecule in the ground singlet electronic state can add to methylacetylene without a barrier producing a three-member or a four-member ring intermediate, which can rapidly rearrange to the most stable  $H_3CCCCCH$  isomer on the  $C_5H_4$  singlet surface. This isomer can then lose a hydrogen atom (H) or molecular hydrogen ( $H_2$ ) from the  $CH_3$  group with the formation of  $H_2CCCCCH$  and  $HCCCCCH$ , respectively. Alternatively, H atom migrations and three-member-ring closure/opening rearrangements followed by H and  $H_2$  losses can lead to other isomers of the  $C_5H_3$  and  $C_5H_2$  species. According to the calculated energetics, the  $C_2(X^1\Sigma_g^+) + CH_3CCH$  reaction is likely to be a major source of the  $C_5H_3$  radicals (in particular, the most stable  $H_2CCCCCH$  and  $HCCCHCCH$  isomers, which are relevant to the formation of benzene through the reactions with  $CH_3$ ). Among heavy-fragment product channels, only  $C_3H_3 + C_2H$  and  $c-C_3H_2 + C_2H_2$  might compete with  $C_5H_3 + H$  and  $C_5H_2 + H_2$ . RRKM calculations of reaction rate constants and product branching ratios depending on the reactive collision energy showed that the major reaction products are expected to be  $H_2CCCCCH + H$  (64–66%) and  $HCCCHCCH + H$  (34–30%), with minor contributions from  $HCCCCCH + H_2$  (1–2%),  $HCCCHCC + H_2$  (up to 1%),  $C_3H_3 + C_2H$  (up to 1%), and  $c-C_3H_2 + C_2H_2$  (up to 0.1%) if the energy randomization is complete. The calculations also indicate that the  $C_2(X^1\Sigma_g^+) + CH_3CCH(X^1A_1)$  reaction can proceed by direct H-abstraction of a methyl hydrogen to form  $C_3H_3 + C_2H$  almost without a barrier.

## 1. Introduction

The dicarbon molecule,  $C_2$ , is ubiquitous in various environments and has been detected in hydrocarbon flames,<sup>1–3</sup> in chemical vapor deposition of diamond,<sup>4</sup> and in the interstellar medium, including cold molecular clouds,<sup>5</sup> circumstellar envelopes,<sup>6</sup> and cometary comae.<sup>7–9</sup> Therefore, gas-phase reactions of  $C_2$  are believed to play an important role in the chemistry of those environments. For example, John et al.,<sup>4</sup> Shiomi et al.,<sup>10</sup> and others<sup>11,12</sup> suggested that dicarbon is the actual precursor in the formation of nanocrystalline diamond; number densities in  $H_2/Ar/CH_4$  plasmas have been determined on the order of  $10^{13} \text{ cm}^{-3}$ . These processes are closely related to the growth of carbon clusters in carbon-rich stars<sup>13</sup> as well as to the synthesis of diamonds in hydrogen-poor preplanetary nebulae<sup>14</sup> and in our solar system.<sup>15</sup> In hydrocarbon combustion, dicarbon molecules are important as potential precursors to polycyclic aromatic hydrocarbons (PAHs) and to their hydrogen deficient precursor molecules and small carbon-bearing radicals.<sup>16–18</sup> Synthetic routes are proposed via sequential addition steps of ground-state atomic carbon, carbon molecules ( $C_2$  and  $C_3$ ), and small hydrocarbon radicals to unsaturated hydrocarbons eventually leading to PAH-like structures and fullerenes.<sup>19–23</sup> In particular, the reactions of  $C_2$  are expected to open prompt routes to form hydrocarbon radicals with multiple carbon–carbon bonds, including resonance-stabilized free radicals (RSFRs) such as  $C_4H_3$  and  $C_5H_3$ . These radicals are believed to play an important

role in the formation of aromatic compounds, PAHs, and soot in the combustion of aromatic fuels.<sup>24,25</sup> Owing to electron delocalization, RSFRs are more stable than ordinary radicals, are relatively unreactive, and can reach a high concentration in flames. These high concentrations and the relatively fast rates of the RSFR + RSFR reactions make them an important mechanism to form complex hydrocarbons in flames. Therefore, it is necessary to investigate the reaction mechanisms, absolute rate constants, and product branching ratios for possible reactions producing RSFRs and to include these reactions into combustion chemistry networks.

Due to their importance, the kinetics of reactions involving the ground electronic  $X^1\Sigma_g^+$  state of  $C_2$  and also the excited  $a^3\Pi_u$  state have been extensively investigated by following the  $C_2(X^1\Sigma_g^+, a^3\Pi_u)$  disappearance in the presence of various collision partners.<sup>26–30</sup> The reactions of the ground-state  $C_2$  with unsaturated hydrocarbons were found to be of the gas kinetic order. However, despite this wide kinetic investigation, information on the reaction products, their branching ratios depending on the reaction conditions, and involved intermediates is still scarce. In some cases, primary products and reaction mechanisms were speculated on the basis of the observed temperature dependence of the reactions. Only recent crossed molecular beam experiments by Kaiser's group performed under single collision conditions combined with our electronic structure calculations<sup>31–34</sup> were able to shed some light on the reaction mechanism at the microscopic level and identify the primary products without the occurrence of collisional stabilization of the involved intermediates or secondary reactions. The results

<sup>†</sup> Florida International University.

<sup>‡</sup> University of Hawaii at Manoa.

indicated that the reactions of  $C_2(X^1\Sigma_g^+, a^3\Pi_u)$  with ethylene mostly produce  $C_4H_3$  radicals<sup>31,32</sup> and those with acetylene give the 1,3-butadiynyl,  $C_4H(X^2\Sigma^+)$ , + H products.<sup>33,34</sup> Thus, the reactions of dicarbon molecules with alkenes and alkynes are likely to be dominated by the  $C_2$ -for-H exchange channel. If this is still the case for the reaction of  $C_2$  with methylacetylene,  $CH_3CCH$ , the expected major reaction products should be  $C_5H_3$  + H. This would make the  $C_2 + CH_3CCH$  reaction of special significance for the formation of the first aromatic ring in combustion flames and the interstellar medium, as the  $C_5H_3$  radicals were demonstrated to play an important role in the production of benzene through their reaction with  $CH_3$ <sup>25,35,36</sup> and the dicarbon and methylacetylene molecules are present in both environments.

The present paper is devoted to a theoretical study of the potential energy surface (PES) of the reaction of dicarbon in its ground  $X^1\Sigma_g^+$  electronic state with  $CH_3CCH(X^1A_1)$  with the goal to unravel the reaction mechanism, to elucidate potential intermediates involved in the reaction, and to predict reaction products. The PES and molecular parameters of various species are used for microcanonical RRKM calculations of rate constants for individual reaction steps depending on collision energy. The rate constants are then utilized to compute branching ratios of various products. The present theoretical study precedes future experimental measurements of the  $C_2(X^1\Sigma_g^+) + CH_3CCH(X^1A_1)$  reaction in crossed molecular beams. Theory and experiment will complement each other and will eventually help to unravel the details of collision-energy-dependent chemical dynamics, reaction rate constants, and relative yields of various products of this reaction.

## 2. Computational Methods

The geometries of the reactants, products, intermediates, and transition states have been optimized by employing the hybrid density functional B3LYP method<sup>37,38</sup> with the 6-311G(d,p) basis set. Vibrational frequencies, calculated at the same B3LYP/6-311G(d,p) level, were used for characterization of the stationary points (number of imaginary frequencies NIMAG = 0 and 1 for local minima and transition states, respectively) and zero-point energy corrections (ZPE). To obtain more accurate energies, we used the G2M(RCC,MP2) computational scheme,<sup>39</sup> which approximates coupled cluster RCCSD(T) calculations<sup>40</sup> with the large 6-311+G(3df,2p) basis set. The G2M(RCC,MP2)/B3LYP/6-311G(d,p) + ZPE[B3LYP/6-311G(d,p)] calculational approach is expected to provide accuracies of 1–2 kcal/mol for relative energies of various stationary points on PES including transition states, unless a wave function has a strong multireference character. The closed-shell singlet wave functions of key transition states were tested on the subject of their instability with respect to an open-shell character. Normally, no such instability was detected supporting mostly a single-reference character of the wave functions. The only exception was the transition state for the direct H abstraction,  $C_2(X^1\Sigma_g^+) + CH_3CCH \rightarrow C_2H(X^2\Sigma^+) + CH_2CCH(^2B_1)$ , which indeed exhibits a strong multireference nature. Hence, that transition state was optimized at the CASSCF/6-311G(d,p) level,<sup>41</sup> and its relative energy was refined using the MRCI/6-311+G(3df,2p) method.<sup>42</sup> The GAUSSIAN 98<sup>43</sup> and MOLPRO 2002<sup>44</sup> programs were employed for the calculations.

We used RRKM theory for computations of rate constants of individual reaction steps.<sup>45–47</sup> Rate constant  $k(E)$  at an internal energy  $E$  for a unimolecular reaction  $A^* \rightarrow A^\# \rightarrow P$  can be expressed as

$$k(E) = \frac{\sigma W^\#(E - E^\#)}{h} \rho(E)$$

where  $\sigma$  is the reaction path degeneracy,  $h$  is Plank's constant,  $W^\#(E - E^\#)$  denotes the total number of states for the transition state (activated complex)  $A^\#$  with a barrier  $E^\#$ ,  $\rho(E)$  represents the density of states of the energized reactant molecule  $A^*$ , and  $P$  is the product or products. We employed the harmonic approximation to calculate the total number and density of states. For the case in which the excitation energy is large and there exist low-frequency modes, the harmonic approximation will not be accurate for low-frequency modes in calculating these quantities and may introduce certain errors in our treatment. To take into account anharmonicity, more sophisticated RRKM calculations are required, but they are beyond the scope of the present work.

For the reaction channels, which do not exhibit exit barriers, we applied the microcanonical variational transition state theory (VTST)<sup>47</sup> and thus determined variational transition states and rate constants. In the microcanonical VTST, the minimum in the microcanonical rate constant is found along the reaction path according to the following equation

$$\frac{dk(E)}{dq^\#} = 0$$

where  $q^\#$  is the reaction coordinate, so that a different transition state is found for each different energy. The individual microcanonical rate constants were minimized at the point along the reaction path where the sum of states  $W^\#(E - E^\#)$  has a minimum. Each of these calculations requires values of the classical potential energy, zero-point energy, and vibrational frequencies as functions of the reaction coordinate. We used the following procedure for the VTST calculations. At first, we calculated a series of energies at different values of the reaction coordinate in question. To obtain these energies, we performed partial B3LYP/6-31G\*\* geometry optimization with fixed values of the reaction coordinate and all other geometric parameters being optimized. The unrestricted UB3LYP theoretical level was used for these calculations because VTSSs are typically observed for single-bond cleavage processes, in which a closed-shell singlet wave function of a reactant converts into an open-shell singlet (doublet + doublet) wave function of products. Then, we calculated  $3N - 7$  vibrational frequencies projecting the reaction coordinate out. Single-point energies for the optimized structures were refined at the coupled cluster UCCSD(T)/6-311G\*\* level. Then, the UCCSD(T)/6-311G\*\* energies were multiplied by a scaling factor in order to match UCCSD(T)/6-311G\*\* and G2M energies of the final dissociation products. The scaling factor in this procedure was computed as the ratio of the relative energies of the products calculated at the G2M and UCCSD(T)/6-311G\*\* levels.

Assuming single-collision conditions for the reaction, master equations for unimolecular reactions can be expressed as follows:

$$\frac{d[C]_i}{dt} = \sum k_n [C]_j - \sum k_m [C]_i$$

where  $[C]_i$  and  $[C]_j$  are concentrations of various intermediates or products, and  $k_n$  and  $k_m$  are microcanonical rate constants computed using the RRKM theory. Only a single total-energy level was considered throughout, as for single-collision crossed-beam conditions. We used the steady-state approximation to

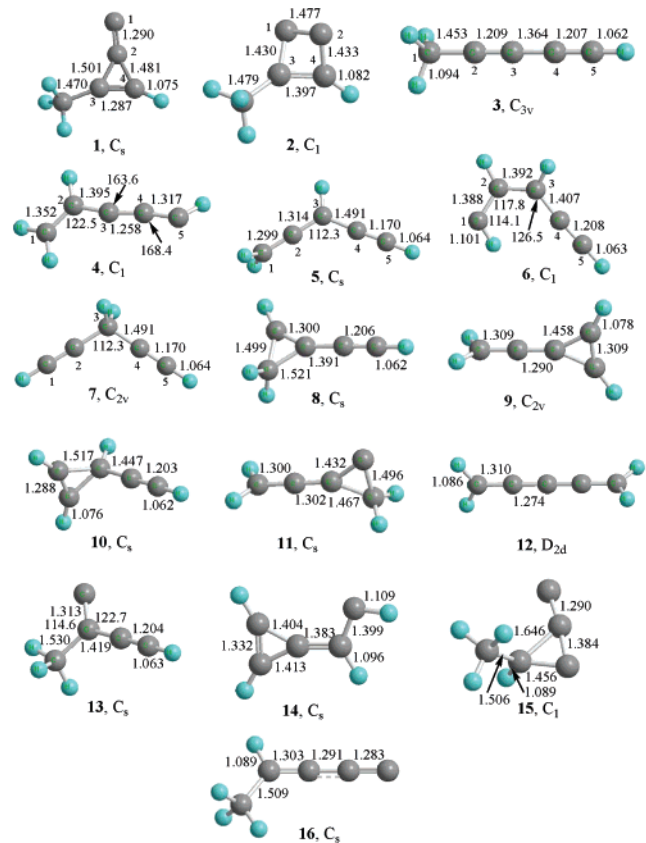


**Figure 1.** Geometries of various  $C_5H_4$  intermediates of the  $C_2(X^1\Sigma_g^+)$  +  $CH_3CCH(X^1A_1)$  reaction optimized at the B3LYP/6-311G(d,p) level. Selected bond lengths and bond angles are given in angstroms and degrees, respectively.

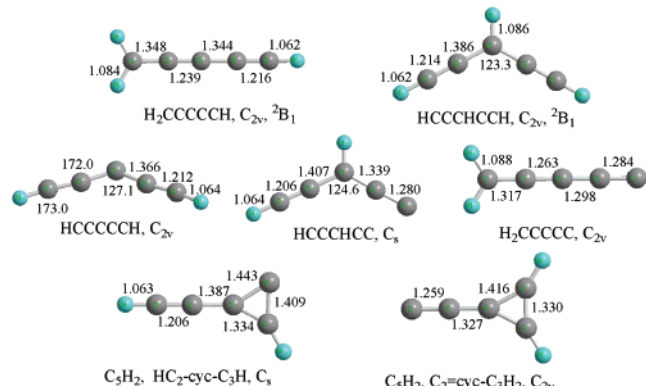


**Figure 2.** Geometries of various  $C_5H_3$  and  $C_5H_2$  products of the  $C_2(X^1\Sigma_g^+)$  +  $CH_3CCH(X^1A_1)$  reaction optimized at the B3LYP/6-311G\*\* level. Selected bond lengths and bond angles are given in angstroms and degrees, respectively.

solve the system of master equations and to compute the product branching ratios.

### 3. Results and Discussion

**3.1. Potential Energy Surface.** Optimized structures of various intermediates, products, and transition states in the  $C_2(X^1\Sigma_g^+)$  +  $CH_3CCH$  reaction are shown in Figures 1–3, respectively. The most important bond lengths and bond angles are also shown in these Figures. Optimized Cartesian coordinates and vibrational frequencies of all species are presented in Supporting Information.

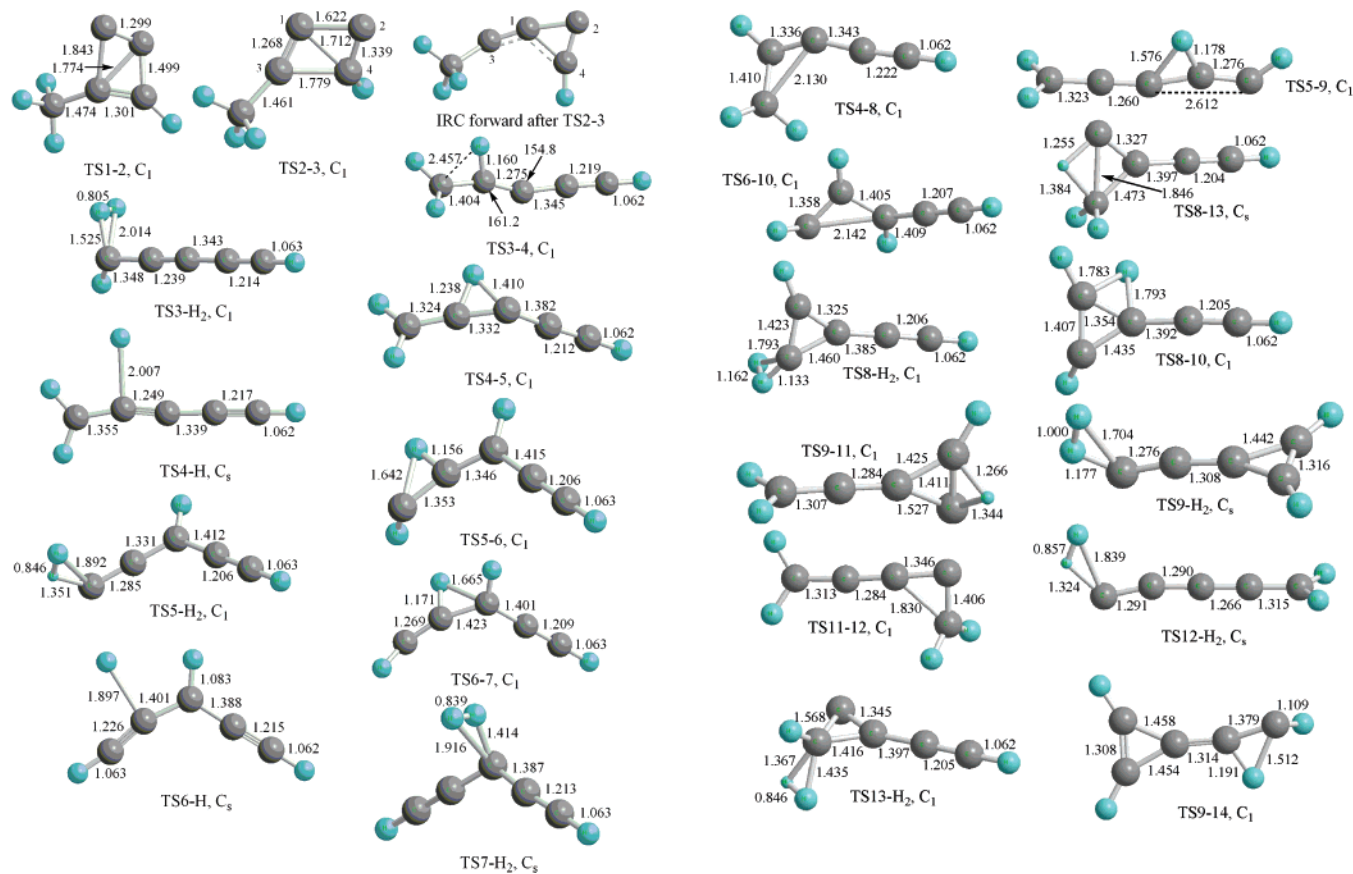
**Entrance Reaction Channel.** As seen on the schematic potential energy diagram (Figure 4), when a singlet  $C_2$  molecule

adds to methylacetylene, two different  $C_5H_4$  isomers can be initially produced. The first one is intermediate **1**, which has a  $C_s$ -symmetric three-member ring structure with external (out-of-ring) C and H atoms and a  $CH_3$  group. Species **1** resides 70.9 kcal/mol below the  $C_2(X^1\Sigma_g^+)$  +  $CH_3CCH$  reactants and is formed by barrierless addition of the  $C_2$  molecule to the triple  $\equiv C$  bond of methylacetylene in an end-to-side manner. To verify that this addition proceeds without a barrier, we scanned the PES using the  $C-X$  distance between the carbon atom in  $C_2$  and the center of the  $\equiv C$  bond as a reaction coordinate, keeping the two CC bonds perpendicular to each other, and optimizing all other geometric parameters. The resulting potential energy profile calculated at the B3LYP/6-311G(d,p) level is illustrated in Figure 5a. As one can see, the energy smoothly and monotonically decreases as the  $R_{C-X}$  distance changes from 4.0 to 1.2 Å confirming that no barrier exists on the reaction path, at least at the present level of theory. If the constraint for the two CC bonds to be perpendicular to each other is lifted, the energies of the structures on the minimal energy reaction path (MEP) can only lower; in any case, the PES plot in Figure 5a demonstrates an existence of a barrierless trajectory from the reactants to intermediate **1**.

The second possible initial reaction intermediate is a four-member ring structure **2** produced by side-to-side addition of  $C_2$  to the acetylenic bond of  $CH_3CCH$  and lying 70.5 kcal/mol lower in energy than the reactants. Again, we have confirmed that this addition occurs without an entrance barrier. The potential energy profile was scanned with the  $X_1-X_2$  distance between the centers of two C–C bonds (Figure 5b) serving as a reaction coordinate. The two bonds were kept perpendicular to the  $X_1-X_2$  axis, and other geometric parameters were optimized. The potential energy shows a steady decrease from the reactants to the vicinity of intermediate **2**, and therefore, no barrier exists for the side-to-side addition. Again, if one performs the PES scan without the restriction for the two bonds to be perpendicular to the  $X_1-X_2$  axis, the energies of MEP structures can only decrease. Regardless of the constraint used during the geometry optimization, the PES plot in Figure 5b shows a trajectory leading from  $C_2(X^1\Sigma_g^+)$  +  $CH_3CCH$  to **2** without a barrier.

Interestingly, the structures similar to isomers **1** and **2** were found earlier as initial intermediates in the reaction of singlet dicarbon with acetylene.<sup>33,34</sup> Relative energies of the three- and four-member ring intermediates in the  $C_2(X^1\Sigma_g^+)$  +  $C_2H_2$  reaction are –68.9 and –68.1 kcal/mol, respectively, close to the values calculated here for **1** and **2**. Therefore, the replacement of a hydrogen atom with a methyl group does not significantly affect the geometry and energetics of these isomers. The four-member ring in intermediate **2** is nonplanar with the dihedral CCCC angle of 39.2°, and the bonding character is apparently best described by a double bond between  $C_3$  and  $C_4$ , single  $C_1-C_3$ ,  $C_2-C_4$ , and  $C_1-C_2$  bonds, and carbene lone pairs on the  $C_1$  and  $C_2$  atoms. Other resonance configurations also contribute to the electronic structure, as the  $C_1-C_3$  and  $C_2-C_4$  distances are too short for single bonds (~1.43 Å) and  $C_3-C_4$  is too long for a double bond (~1.40 Å). On the other hand, the bonding character of **1** is straightforward and is described by double  $C_1=C_2$  and  $C_3=C_4$  and single  $C_2-C_3$  and  $C_2-C_4$  bonds, and a lone pair on  $C_1$ . Intermediates **1** and **2** are separated by a relatively low, ~15 kcal/mol, barrier for ring extension at TS1-2, which lies 55.2 kcal/mol below the reactants.

At the next reaction step, **2** can isomerize to the most stable singlet  $C_5H_4$  intermediate **3**,  $C_{3v}$ -symmetric methyldiacetylene  $H_3C-C\equiv C-C\equiv C-H$ , residing 137.6 kcal/mol lower in energy



with respect to  $\text{C}_2(^1\Sigma_g^+) + \text{CH}_3\text{CCH}$ . It seems that this rearrangement can proceed by a simple cleavage of the  $\text{C}_3=\text{C}_4$  bond in **2**; however, it appears to be more complicated. In the corresponding transition state **TS2-3**, the  $\text{C}_3-\text{C}_4$  bond starts to break (as this distance elongates to 1.78 Å), but a new  $\text{C}_1-\text{C}_4$  begins to form (1.71 Å), see Figure 3. According to intrinsic reaction coordinate (IRC)<sup>48</sup> calculations, after the barrier at **TS2-3** is cleared, a three-member structure with a  $\text{C}_1\text{C}_2\text{C}_4$  ring is formed, where the  $\text{CCH}_3$  group and H are linked to the  $\text{C}_3$  and  $\text{C}_4$  atoms, respectively (see the “IRC forward after **TS2-3**” structure in Figure 3). However, this structure is not a local minimum, and on the further course of IRC calculations the  $\text{C}_1-\text{C}_2$  bond breaks and the hydrogen atom migrates from  $\text{C}_4$  to  $\text{C}_2$  eventually leading to the formation of intermediate **3**. Full details of the IRC calculations are given in Supporting Information. The barrier separating **2** and **3** is calculated to be relatively low, 21.4 kcal/mol, as **TS2-3** lies 49.1 kcal/mol below the reactants. Therefore, we can expect that methyldiacetylene **3** can be rapidly produced from the reactants if the initial intermediates **1** and **2** are not collisionally deactivated, for instance, in combustion flames and in high-density cometary comae.

An interesting question to address is whether the dicarbon molecule can directly insert into the single  $\text{C}-\text{C}$  or acetylenic  $\text{C}-\text{H}$  bonds of  $\text{CH}_3\text{CCH}$  to immediately produce the highly exothermic isomer **3**. To answer this question, we calculated the MEP for would-be insertions of  $\text{C}_2$  into the  $\text{C}-\text{C}$  and  $\text{C}-\text{H}$  bonds. For the  $\text{C}-\text{C}$  case, the MEP was obtained by scanning the entrance PES using the  $\text{C}-\text{X}$  distance between the attacking carbon atom of  $\text{C}_2$  and the  $\text{C}-\text{C}$  bond center X as a reaction coordinate, keeping the  $\text{C}-\text{C}$  bond perpendicular to the  $\text{C}-\text{X}$  axis, and allowing all other parameters to be optimized (see Figure 5c). Initially, as  $\text{C}_2$  approaches the center of the single  $\text{C}-\text{C}$  bond, the potential energy slightly decreases reaching a

shallow minimum at  $R(\text{C}-\text{X}) \approx 2.5$  Å and then increases and exceeds the energy of the reactants with a maximum approximately at 1.8 Å. After that, the energy goes down, but the insertion does not occur. Instead, upon partial geometry optimization, an H atom from the  $\text{CH}_3$  group migrates to the  $\text{C}_2$  fragment, and a  $\text{C}_3$  ring is formed, but the single  $\text{C}-\text{C}$  bond does not break. Because geometry optimization carried in such a way is not full, the structures shown in Figure 5c do not correspond to stationary points on PES. Nevertheless, these results illustrate that energetically favorable trajectories leading from the reactants to intermediate **3** via the insertion of  $\text{C}_2$  into  $\text{C}-\text{C}$  do not exist. When we push the  $\text{C}_2$  fragment toward the center of the acetylenic  $\text{C}-\text{H}$  bond (Figure 5d), the insertion into this bond also does not take place. Initially, the potential energy decreases and a three-member ring structure similar to intermediate **1** is formed. However, if we continue this push closer to the center of the  $\text{C}-\text{H}$  bond, the energy sharply increases. When the MEP scans are performed without the artificial restrictions that the  $\text{C}-\text{X}$  axis is perpendicular to the single  $\text{C}-\text{C}$  or acetylenic  $\text{C}-\text{H}$  bonds being attacked, the attacking  $\text{C}_2$  molecule slips toward the triple  $\text{C}\equiv\text{C}$  bond during the optimization. In this case, instead of the desired insertion into the  $\text{C}-\text{C}$  or  $\text{C}-\text{H}$  bonds, the MEP collapses onto the pathway of the  $\text{C}_2$  addition to the acetylenic  $\text{C}\equiv\text{C}$  bond.

**Rearrangement and Fragmentation of Chain  $\text{C}_5\text{H}_4$  Intermediates.** As seen in Figure 4, the fate of the methyldiacetylene isomer **3** can be threefold. First, it can lose a hydrogen atom from the  $\text{CH}_3$  group and yield the  $\text{H}_2\text{CCCCCH}(\text{C}_{2v}, ^2\text{B}_1) + \text{H}$  products without an exit barrier. The H elimination is calculated to be 91.6 kcal/mol endothermic; however, the products reside 46.0 kcal/mol below the initial  $\text{C}_2(^1\Sigma_g^+) + \text{CH}_3\text{CCH}$  reactants. A loss of the acetylenic hydrogen is much less favorable. Our earlier calculations of various  $\text{C}_5\text{H}_3$  isomers showed that the  $\text{H}_3\text{CCCCC}(\text{C}_{s2}, ^2\text{A}')$  structure lies about 41 kcal/mol above

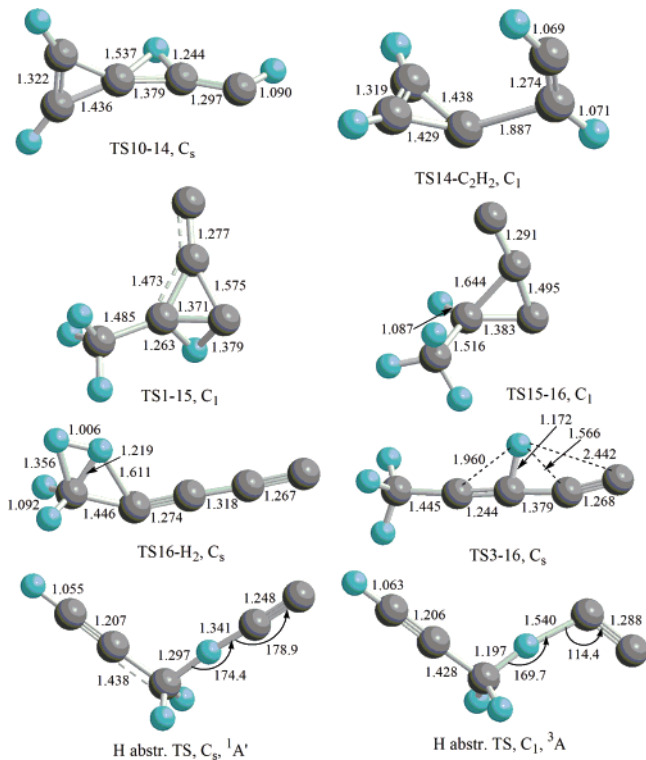


**Figure 3.** Geometries of various transition states on the singlet  $C_5H_4$  PES optimized at the B3LYP/6-311G\*\* level. Selected bond lengths and bond angles are given in angstroms and degrees, respectively.

$H_2CCCCCH$ .<sup>35</sup> Therefore, although the  $C_2(^1\Sigma_g^+) + CH_3CCH \rightarrow 3 \rightarrow H_3CCCCC + H$  reaction would be slightly exothermic, it is unfavorable kinetically. The second possible dissociation channel of methyldiacetylene is  $H_2$  elimination from the  $CH_3$  group. This leads to the formation of the  $H_2CCCCCH(C_{2v}, ^1A_1)$  molecule overcoming a barrier of 99.9 kcal/mol at TS3- $H_2$ . The  $H_2CCCCCH(C_{2v}, ^1A_1) + H_2$  products reside 50.0 kcal/mol below  $C_2(^1\Sigma_g^+) + CH_3CCH$  and 4.0 kcal/mol lower in energy than  $H_2CCCCCH(C_{2v}, ^2B_1) + H$ . However, the exit barrier for the  $H_2$  elimination from **3** is 8.3 kcal/mol higher than the energy required to split an atomic hydrogen from the  $CH_3$  group. The third possibility is 1,2-migration of a  $CH_3$  hydrogen to the neighboring C atom, which results in the nonsymmetric intermediate  $H_2CCHCCCH$  **4**. Structure **4** is 52.9 kcal/mol less stable than **3**, and the barrier for the H shift at TS3-4 is calculated to be 73.9 kcal/mol.

Next, intermediate **4** can eliminate the hydrogen atom from the carbon in position 2; H losses from the other C atoms are unfavorable in terms of the product energies. The  $H_2CCHCCCH$  **4**  $\rightarrow H_2CCCCCH + H$  reaction is 38.7 kcal/mol endothermic and exhibits an exit barrier of 2.9 kcal/mol at TS4- $H$ . Although the reverse reaction is recombination of two radicals, it has a barrier. The existence of this barrier can be attributed to two factors: first, the fact that the H atom adds to  $C_2$  but the unpaired electron (the radical site) in  $H_2CCCCCH$  is located on  $C_1$ , and second, a relatively low exothermicity of the recombination reaction. Thus, a H atom can add to the  $C_1$  position of  $H_2CCCCCH$  without a barrier and with the energy gain of 91.6 kcal/mol or to the  $C_2$  position with exothermicity of only 38.7 kcal/mol and overcoming a barrier of 2.9 kcal/mol. Alternatively to the H loss, **4** can undergo a second, 2,3-H shift to the central carbon  $C_3$ . The corresponding barrier at TS4-5 is rather low, 12.9 kcal/mol, and the migration results in much more stable intermediate **5**,  $H_2CCCHCCCH$ . The latter lies 132.5 kcal/mol below the reactants and is only 5.1 kcal/mol less stable than

methyldiacetylene. Structure **5** can eliminate H atoms from  $C_3$  and  $C_1$  to produce the  $H_2CCCCCH$  and  $HCCCHCCH(C_{2v}, ^2B_1)$  isomers of the  $C_5H_3$  radical, respectively, without exit barriers. The energy difference between the two products is only 0.3 kcal/mol at the G2M(RCC,MP2) level, and the two H eliminations from  $H_2CCCCCH$  are endothermic by 86.5 and 86.8 kcal/mol, respectively. A molecular hydrogen can be also split from the  $CH_2$  group in **5** via a barrier of 92.4 kcal/mol at TS5- $H_2$ . Then, the  $HCCCHCCH(C_3)$  isomer of  $C_5H_2$  is formed with endothermicity of 81.6 kcal/mol; the  $HCCCHCCH + H_2$  products reside 50.9 kcal/mol lower in energy than the initial reactants. Finally, a third, 1,2-H shift in **5** gives the  $HCCH-CHCCH$  intermediate **6** over a barrier of 64.4 kcal/mol.

The  $HCCH-CHCCH$  intermediate, 76.3 kcal/mol below  $C_2(^1\Sigma_g^+) + CH_3CCH$ , can split the H atom from  $C_2$  leading to the  $HCCCHCCH$  product. As in the case of intermediate **4**, the exothermicity of the H elimination from **6** is relatively low, 30.6 kcal/mol, and the reaction exhibits an exit barrier. If we consider the reverse recombination of the  $HCCCHCCH$  radical with H, the hydrogen atom can add to  $C_1$  (and, as seen below, to  $C_3$ ) without barriers and with high exothermicities; however, its addition to  $C_2$  requires overcoming a barrier of 3.9 kcal/mol. The 2,3-H shift in **6** occurs via a barrier of only 13.5 kcal/mol and leads to the much more stable  $C_5H_4$  intermediate **7**,  $C_{2v}$ -symmetric  $HCCCH_2CCH$ , which resides 127.8 kcal/mol below the reactants. Formally, this intermediate could be directly produced from the initial reactants by insertion of the attacking  $C_2$  molecule into a methyl C–H bond. However, similar to the insertions into C–C and acetylenic C–H bonds, we could not find a direct and energetically favorable trajectory leading from  $C_2 + CH_3CCH$  to  $HCCCH_2CCH$ . A scan of PES along the minimal energy reaction path for the  $C_2$  approaching methylacetylene from the  $CH_3$  group side performed without any additional constraints showed that, initially, the energy increases above that of the reactants. As the dicarbon molecule approaches close enough to one of the hydrogen atoms in the methyl group, this H atom transfers to  $C_2$ , and only then the energy starts to decrease. A search for a first-order saddle point on this pathway failed; instead, a transition state was found in this vicinity for the abstraction reaction,  $C_2(X^1\Sigma_g^+) + CH_3CCH \rightarrow C_2H(^2\Sigma^+) + CH_2CCH(^2B_1)$ , which will be described in a subsequent section. This result indicates that the insertion is not likely to occur and the  $HCCCH_2CCH$  structure can be formed only through a multistep mechanism following the barrierless addition of  $C_2$  to the acetylenic bond of  $CH_3CCH$ . Species **7** can fragment by the H loss from  $C_3$  to produce  $HCCCHCCH$  without an exit barrier or by  $H_2$  elimination from the same carbon atom to form the bent  $C_{2v}$ -symmetric  $HCCCCCH$  isomer of  $C_5H_2$  over a barrier of 91.1 kcal/mol.

**Pathways Involving Three-Member Ring Intermediates and Their Dissociation Channels.** In addition to H migrations,  $C_5H_4$  intermediates can rearrange through ring-opening/closure processes. A potential energy diagram showing such isomerization pathways involving structures with three-member rings is illustrated in Figure 6. For instance, intermediate **4** can easily undergo ring closure to **8** with the barrier and exothermicity of 2.0 and 28.9 kcal/mol, respectively. A ring closure of structure **5** leading to intermediate **9** is less favorable and goes over a barrier of 64.4 kcal/mol. On the other hand, **6** is only metastable with respect to the ring-closure rearrangement as the barrier separating it from intermediate **10** is as low as 0.2 kcal/mol. Structure **10** can isomerize to a slightly more stable structure by a hydrogen shift between two ring carbons, but the barrier

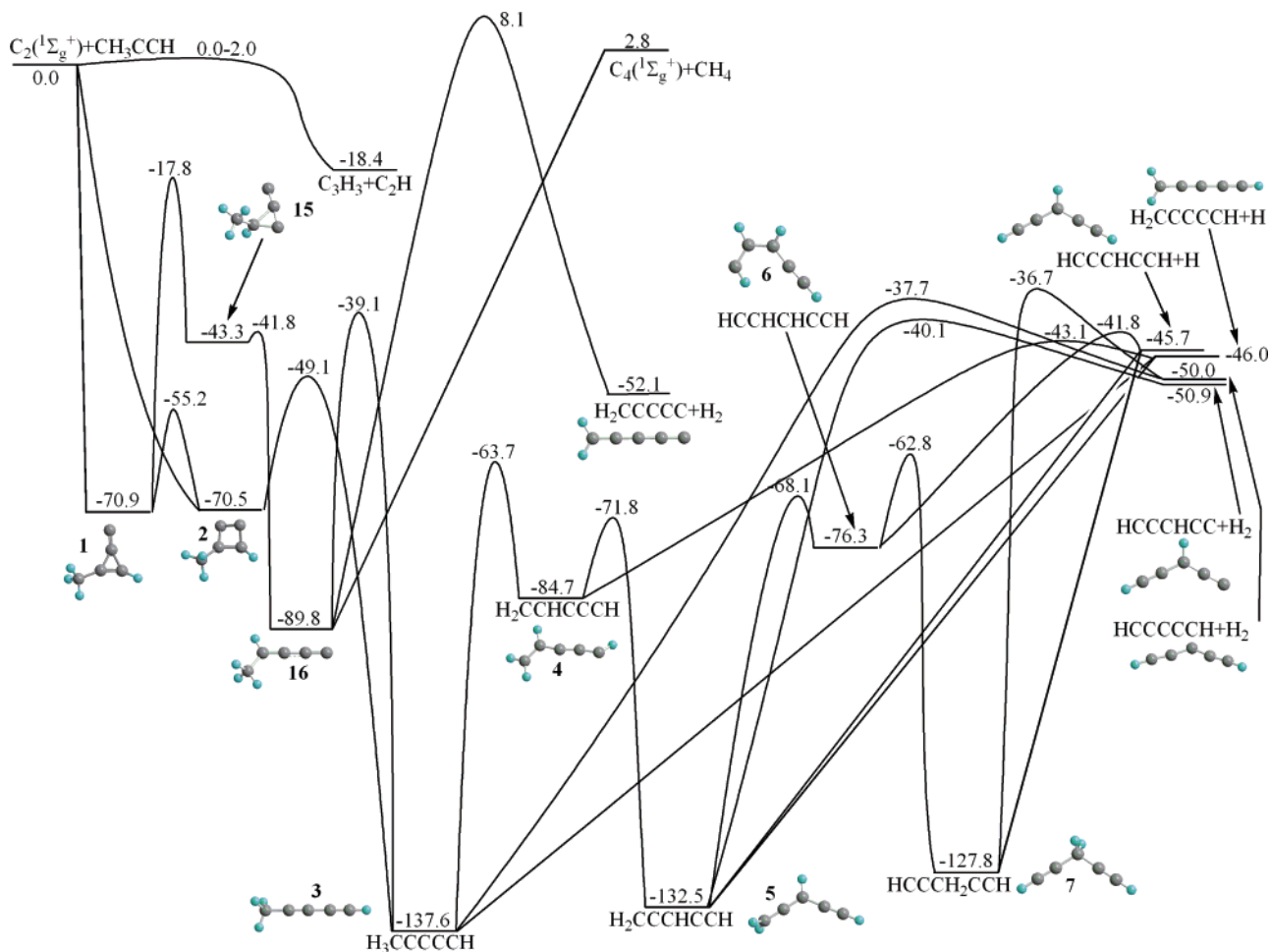


**Figure 4.** Potential energy diagram of the  $\text{C}_2(\text{X}^1\Sigma_g^+)$  +  $\text{CH}_3\text{CCH}(\text{X}^1\text{A}_1)$  reaction calculated at the G2M(RCC,MP2) level. Relative energies of various species are given in kcal/mol.

is high, 88.0 kcal/mol. A similar H shift in **9** leads to a metastable cyclic intermediate **11** over a barrier of 58.6 kcal/mol. Then, **11** readily ring-opens going over an only 0.1 kcal/mol barrier and forming a linear cumulenic  $\text{H}_2\text{CCCCCCH}_2$  intermediate **12**. Finally, the cyclic intermediate **8** can also open its ring and form a branched intermediate **13**. This process is accompanied by the H shift over the ring C–C bond being cleaved and the formation of a terminal  $\text{CH}_3$  group. The **8** → **13** isomerization is 28.1 kcal/mol endothermic and exhibits a barrier of 38.6 kcal/mol. Other ring-closure rearrangement may lead to five-member ring  $\text{C}_5\text{H}_4$  isomers, such as, for example, the ring closure in **12** with formation of the  $\text{CH}_2$ – $\text{CH}_2$  bond. However, such processes are highly unfavorable energetically and are not expected to be relevant to the  $\text{C}_2(\text{X}^1\Sigma_g^+)$  +  $\text{CH}_3\text{CCH}$  reaction, although the reverse five-member ring-opening rearrangements are important for the  $\text{C}_3$  +  $\text{C}_2\text{H}_4$  reaction.<sup>32</sup>

Now we consider various dissociation pathways of intermediates **8**–**13**. Intermediate **8** eliminates  $\text{H}_2$  from the  $\text{CH}_2$  group to form the most stable  $\text{C}_5\text{H}_2$  isomer, ethynylcyclopropenylidene,  $\text{HC}_2\text{-cyc-C}_3\text{H}$ . The relative energy of the ethynylcyclopropenylidene +  $\text{H}_2$  products is −65.6 kcal/mol with respect to the initial reactants, and the barrier for the dissociation of **8** is 84.2 kcal/mol. Species **13** can also decompose to the same  $\text{C}_5\text{H}_2$  isomer by losing  $\text{H}_2$  from the  $\text{CH}_3$  group overcoming a barrier of 64.2 kcal/mol. The  $\text{H}_2$  elimination process in this case is accompanied by closure of a three-member carbon ring. Structure **9** can split  $\text{H}_2$  from the terminal  $\text{CH}_2$  group producing another cyclic  $\text{C}_5\text{H}_2$  isomer,  $\text{C}_2=\text{cyc-C}_3\text{H}_2$ , overcoming a 83.7 kcal/mol barrier.  $\text{C}_2=\text{cyc-C}_3\text{H}_2$  is 18.9 kcal/mol less stable

than ethynylcyclopropenylidene, and the  $\text{C}_2=\text{cyc-C}_3\text{H}_2$  +  $\text{H}_2$  products reside 46.7 kcal/mol below  $\text{C}_2(\text{X}^1\Sigma_g^+)$  +  $\text{CH}_3\text{CCH}$ . The  $\text{H}_2\text{CCCCCH}_2$  intermediate **12** can either lose a hydrogen atom to form  $\text{H}_2\text{CCCCCH}$  without an exit barrier and with an energy loss of 84.0 kcal/mol or eliminate  $\text{H}_2$  from one of its  $\text{CH}_2$  groups giving the  $\text{H}_2\text{CCCC}$  structure. In the latter case, the reaction proceeds via a barrier of 91.5 kcal/mol with endothermicity of 77.9 kcal/mol; the overall  $\text{C}_2(\text{X}^1\Sigma_g^+)$  +  $\text{CH}_3\text{CCH} \rightarrow \text{H}_2\text{CCCC} + \text{H}_2$  reaction is 52.1 kcal/mol exothermic. No first-order saddle point was found for 1,5- $\text{H}_2$  elimination from two different  $\text{CH}_2$  groups in **12** to produce  $\text{HCCCCCH} + \text{H}_2$ ; this reaction pathway is clearly unfavorable.

**Dissociation to Heavy Fragments.** Several dissociation channels leading to the formation of two heavy fragments are also possible. They are illustrated in Figure 7. The methyldiacetylene structure **3** can decompose to  $\text{CH}_3$  + linear  $\text{C}_4\text{H}(^2\Sigma^+)$  by the cleavage of the terminal  $\text{H}_3\text{C}$ – $\text{C}$  single bond. The strength of this bond is calculated to be 132.8 kcal/mol, and the  $\text{CH}_3$  +  $\text{C}_4\text{H}$  products are 4.8 kcal/mol exothermic relative to the initial reactants. A rupture of the C–C single bond in **4** gives the  $\text{C}_2\text{H}_3$  + 1– $\text{C}_3\text{H}$  products lying 4.2 kcal/mol above  $\text{C}_2(\text{X}^1\Sigma_g^+)$  +  $\text{CH}_3\text{CCH}$ . The  $\text{C}_3\text{H}_3$  (propargyl radical) +  $\text{C}_2\text{H}$  (ethynyl radical) products, which lie 18.4 kcal/mol lower in energy than the reactants, can be formed by the single C–C bond cleavages either in  $\text{H}_2\text{CCCHCCH}$  **5** or  $\text{HCCCH}_2\text{CCH}$  **7**. All the fragmentation processes mentioned above take place without exit barriers. Another isomer of  $\text{C}_3\text{H}_3$ ,  $\text{H}_3\text{CCC}$ , can be, in principle, produced by the cleavage of the central C–C single bond in methyldiacetylene. However, the  $\text{H}_3\text{CCC}$  structure is known to

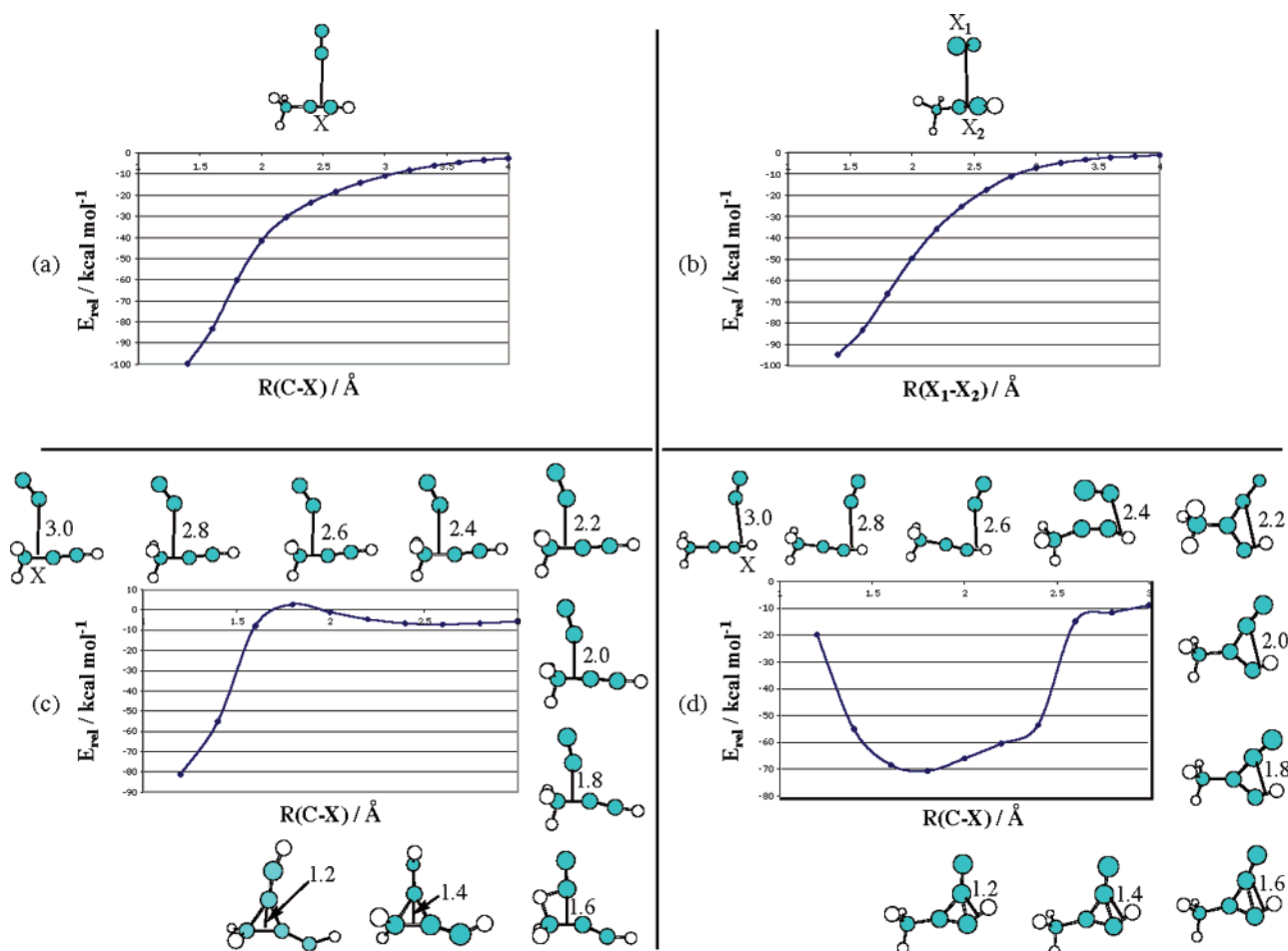


**Figure 5.** Potential energy profiles of minimal energy reaction pathways in the entrance channel of the  $\text{C}_2(\text{X}^1\Sigma_g^+) + \text{CH}_3\text{CCH}(\text{X}^1\text{A}_1)$  reaction: (a) end-to-side addition of  $\text{C}_2$  to the triple  $\text{C}\equiv\text{C}$  bond; (b) side-to-side addition of  $\text{C}_2$  to the triple  $\text{C}\equiv\text{C}$  bond; (c)  $\text{C}_2$  insertion into the single  $\text{C}-\text{C}$  bond; (d)  $\text{C}_2$  insertion into the acetylenic  $\text{C}-\text{H}$  bond.

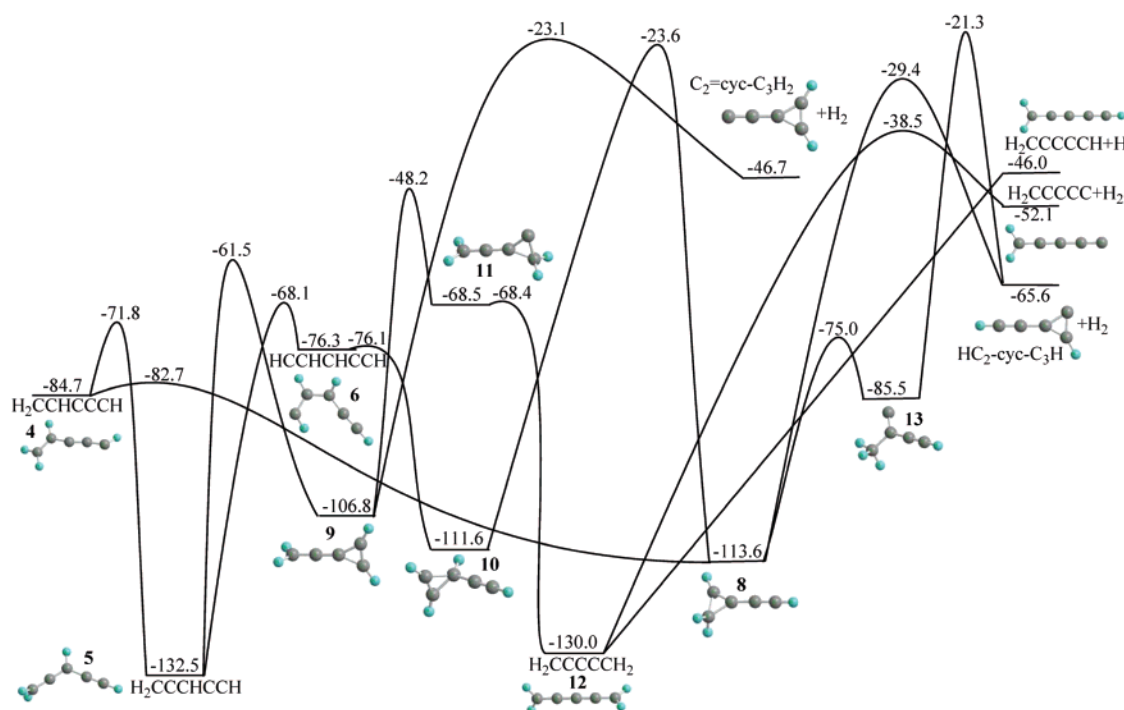


**Figure 6.** Potential energy diagram for the reaction channels involving ring closure/ring opening processes. All relative energies are calculated at the G2M(RCC,MP2) level of theory and given in kcal/mol.

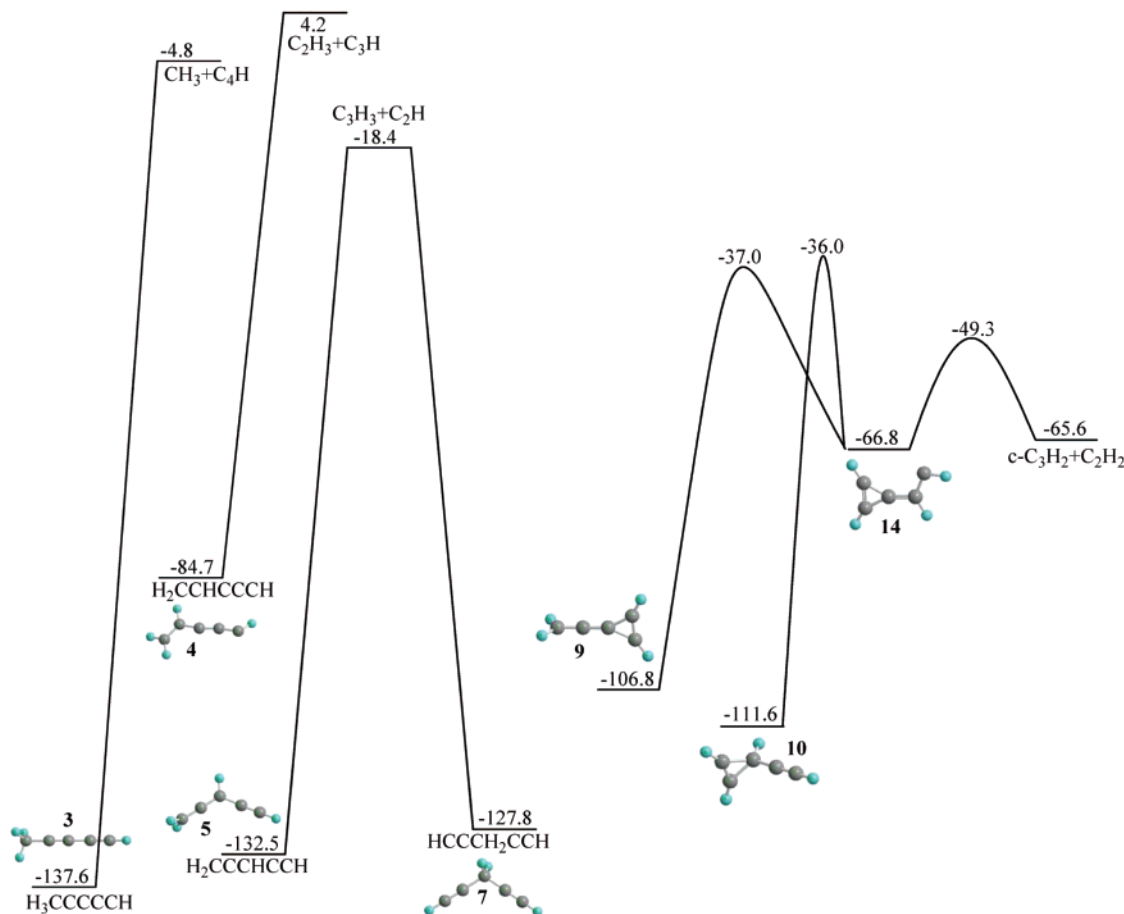


**Figure 7.** Potential energy diagram for the reaction channels leading to various heavy fragments. All relative energies are calculated at the G2M-(RCC,MP2) level of theory and given in kcal/mol.

be  $\sim 40$  kcal/mol less stable than the propargyl radical,<sup>49</sup> so that the  $\text{H}_3\text{CCC} + \text{C}_2\text{H}$  product are expected to be about 22 kcal/mol endothermic. One can see that the single C–C bonds in the  $\text{C}_5\text{H}_4$  isomers are significantly stronger than most of the C–H bonds, and the dissociation processes involving the C–C bond ruptures would not be competitive with H and  $\text{H}_2$  eliminations.

There exists, however, a heavy-fragment decomposition channel, which might be competitive (Figure 7). It leads to the closed-shell  $c\text{-C}_3\text{H}_2$  (cyclopropenylidene) +  $\text{C}_2\text{H}_2$  (acetylene) products, 65.6 kcal/mol exothermic with respect to  $\text{C}_2(^1\Sigma_g^+) + \text{CH}_3\text{CCH}$ , and involves cyclic intermediates **9** and **10**. A 1,2-H shift from the terminal  $\text{CH}_2$  group in **9** occurs with a barrier of 69.8 kcal/mol and leads to another three-member ring intermediate **14**. It can also be produced from intermediate **10** by 1,2-H migration from the ring carbon to the neighboring C of the external CCH group. In this case, the barrier with respect to **10** is 75.6 kcal/mol. Finally, **14** dissociates to  $c\text{-C}_3\text{H}_2 + \text{C}_2\text{H}_2$  by cleaving the exocyclic C=C double bond and overcoming a barrier of 17.5 kcal/mol. Interestingly, together with ethynyl-cyclopropenylidene +  $\text{H}_2$ , cyclopropenylidene + acetylene are the most exothermic products of the  $\text{C}_2(^1\Sigma_g^+) + \text{CH}_3\text{CCH}$  reaction.

Finally, let us consider the reaction pathway leading to the  $\text{C}_4(^1\Sigma_g^+) + \text{CH}_4$  products (Figure 4). It starts from the initial three-member ring intermediate **1**, which undergoes a hydrogen shift between two ring carbons. After the shift depicting a high barrier of 53.1 kcal/mol, another three-member cyclic local minimum **15** is produced. Structure **15** is metastable and can ring-open to the chain intermediate **16**,  $\text{CH}_3\text{C(H)CCC}$ , over-

coming a barrier of only 1.5 kcal/mol. The  $\text{CH}_3\text{C(H)CCC}$  structure is a precursor for  $\text{CH}_4$  elimination, which takes place without an exit barrier. The calculated endothermicity of the  $\text{C}_4(^1\Sigma_g^+) + \text{CH}_4$  products relative to the initial reactants is 2.8 kcal/mol. The reverse reaction, in which a lone pair of a terminal carbon in the electronically excited singlet  $\text{C}_4$  molecule inserts into a C–H bond of methane, is shown to be barrierless. A scan of PES for the minimal energy path for this insertion shows a monotonic energy decrease as  $\text{CH}_4$  approaches the terminal C atom of  $\text{C}_4$  and the C–H bond in methane is broken, while two new C–C and C–H bonds are formed to eventually produce intermediate **16**. The situation here is similar to the  $\text{C}_4(^1\Sigma_g^+) + \text{H}_2$  reaction, which has been also shown to form the singlet  $\text{H}_2\text{CCCC}$  structure without a barrier.<sup>34</sup> The  $^1\Sigma_g^+$  state of  $\text{C}_4$  is an excited electronic state; the ground  $^3\Sigma_g^-$  states lies 10.7 kcal/mol lower in energy making the  $\text{C}_4(^3\Sigma_g^-) + \text{CH}_4$  product channel 7.9 kcal/mol exothermic. However, this channel is spin-forbidden and has to occur via intersystem crossing and therefore is neglected here. The  $\text{CH}_4$  loss is not the only channel for rearrangement or dissociation of  $\text{CH}_3\text{C(H)CCC}$ . It can also lose molecular hydrogen to produce  $\text{H}_2\text{CCCCC} + \text{H}_2$ , but the barrier for such 1,2-H<sub>2</sub> elimination is very high and the corresponding transition state TS16–H<sub>2</sub> lies 8.1 kcal/mol higher in energy than the  $\text{C}_2(^1\Sigma_g^+) + \text{CH}_3\text{CCH}$  reactants. Most likely, however, **16** would isomerize to the methyldiacetylene structure by the 1,4-H shift overcoming a much lower barrier of 50.7 kcal/mol at TS3-16 (39.1 kcal/mol below the reactants). Note that a very similar mechanism (in terms of the structures and energetics of involved intermediates and transition states) leading from **1** to the linear  $\text{XCCCC}$  structure via  $\text{XC(H)CCC}$  was found also

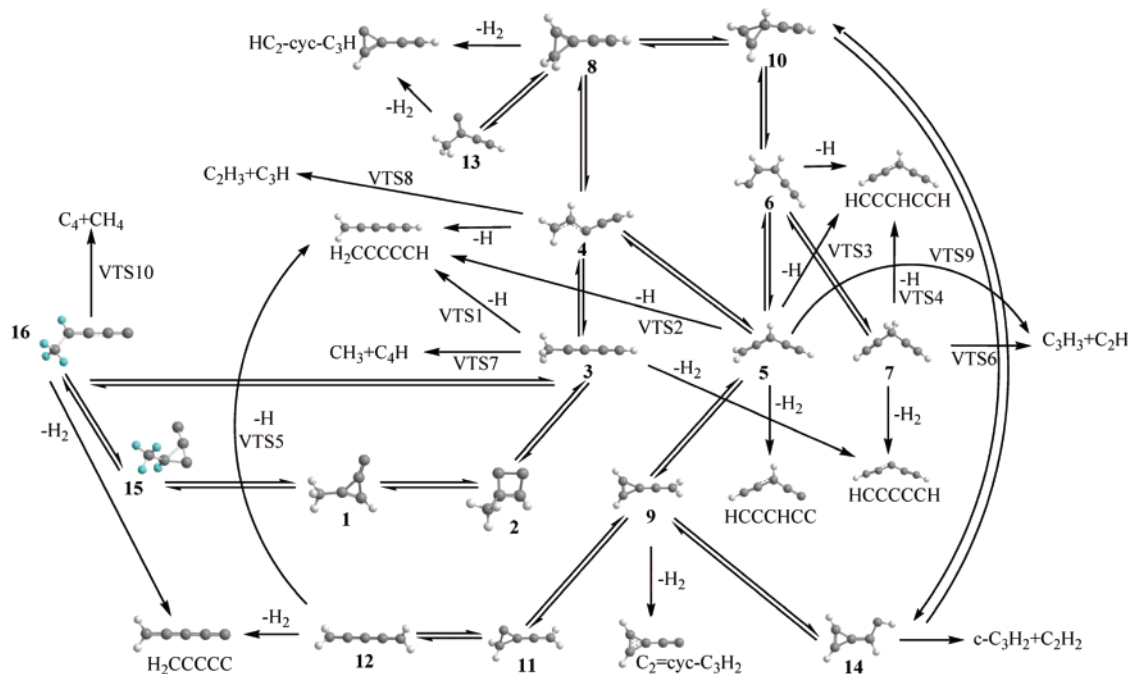


**Figure 8.** Reaction scheme used for the kinetics calculations.

for the  $\text{C}_2(\text{C}_2\text{H}_2)$  reaction,<sup>33,34</sup> where  $X = \text{H}$  instead of  $\text{CH}_3$  as in the present case.

Summarizing, the energized C<sub>5</sub>H<sub>4</sub> isomers formed in the reaction of singlet dicarbon with methylacetylene can decompose by H atom eliminations giving the H<sub>2</sub>CCCCCH and HCCCH-CCH isomers of the C<sub>5</sub>H<sub>3</sub> radical, normally, without exit barriers and with overall reaction exothermicity of about 46 kcal/mol. Second, H<sub>2</sub> eliminations from the C<sub>5</sub>H<sub>4</sub> intermediates can lead to a variety of C<sub>5</sub>H<sub>2</sub> isomers, including ethynylcyclopropenylidene HC<sub>2</sub>-cyc-C<sub>3</sub>H, bent HCCCCCH, HCCCHC, H<sub>2</sub>CCCCC, and C<sub>2</sub>=cyc-C<sub>3</sub>H<sub>2</sub>, for which the reaction exothermicity varies from 65.6 to 46.7 kcal/mol. Although the H<sub>2</sub> loss channels are more exothermic than H eliminations, all of them take place via exit barriers. The relative energies of transition state corresponding to these barriers are in the range 20–40 kcal/mol below the C<sub>2</sub>(<sup>1</sup>Σ<sub>g</sub><sup>+</sup>) + CH<sub>3</sub>CCH reactants; i.e., they lie higher in energy than the C<sub>5</sub>H<sub>3</sub> + H products. Cyclopropanylidene + acetylene are the only highly exothermic heavy-fragment products (−65.6 kcal/mol), but the transition states corresponding to the highest barriers on the pathways leading to c-C<sub>3</sub>H<sub>2</sub> + C<sub>2</sub>H<sub>2</sub> lie only 36–37 kcal/mol lower in energy than the reactants.

*Direct H Abstraction from CH<sub>3</sub>CCH.* The C<sub>3</sub>H<sub>3</sub> + C<sub>2</sub>H products, exothermic by 18.4 kcal/mol, can be achieved by direct hydrogen abstraction from the methyl group by C<sub>2</sub>. Finding a transition state corresponding to this process is a difficult task because the character of the singlet wave function changes from a closed shell for the reactants to an open shell for the products, and a multireference treatment is unavoidable in this case. We optimized the geometry of the abstraction transition state at the CASSCF level with various active spaces ranging from eight electrons distributed on eight orbitals, (8,8), to (14,14). The resulting optimized geometries agree with each other within 0.01–0.02 Å for bond lengths and 1–2° for bond angles. The structure obtained at our best CASSCF(14,14)/6-311G(d,p) level is shown in Figure 3. It has C<sub>s</sub> symmetry and the <sup>1</sup>A' electronic state. The H atom being abstracted is located roughly in the middle between the carbon atom of C<sub>2</sub> and that of the methyl group, and the C<sub>2</sub>HC fragment is nearly linear. The barrier height

refined at the MRCI level, MRCI(14,12)/6-311+G(3df,2p), is only 1.9 kcal/mol. When Davidson corrections for quadruple excitations are taken into account, the barrier height reduces to 0.7 kcal/mol without ZPE, while with ZPE corrections the transition state energy is lower than that of the reactants. Unfortunately, most accurate MRCI calculations with the full-valence active space are not feasible for a molecule of this size. Nevertheless, the present results allow us to conclude that the abstraction reaction should be facile even at low temperatures and can also occur in molecular beams at low collision energies. On the other hand, H abstraction of the acetylenic hydrogen in  $\text{CH}_3\text{CCH}$  is not expected to be competitive because the  $\text{H}_3\text{CCC}$  radical produced in this reaction is  $\sim$ 40 kcal/mol less stable than the propargyl radical,<sup>49</sup> and the abstraction reaction is strongly endothermic.

We have also located the H abstraction transition state from the methyl group in triplet electronic state (see Figure 3) corresponding to the  $\text{C}_2(^3\Pi_u) + \text{CH}_3\text{CCH} \rightarrow \text{C}_2\text{H}(^2\Sigma^+) + \text{CH}_2\text{CCH}(^2\text{B}_1)$  reaction. At the G2M level, the barrier is calculated to be 7.0 kcal/mol relative to the singlet  $\text{C}_2(^1\Sigma_g^+) + \text{CH}_3\text{CCH}$  reactants. Since  $\text{C}_2(^3\Pi_u)$  is about 2 kcal/mol less stable than  $\text{C}_2(^1\Sigma_g^+)$ , the abstraction barrier on the triplet PES is predicted to be  $\sim$ 5 kcal/mol. The entire triplet surface for the  $\text{C}_2(^3\Pi_u) + \text{CH}_3\text{CCH}$  reaction is currently under investigation in our group and will be reported later.

**3.2. Product Branching Ratios.** To quantify branching ratios of various possible  $C_5H_3 + H$ ,  $C_5H_2 + H_2$ , and other products, we carried out microcanonical RRKM calculations of energy-dependent rate constants for individual reaction steps and solved kinetic master equations. However, we have to keep in mind that this treatment assumes a complete energy randomization, which is not necessarily the case in reactive intermediates formed in the  $C_2(^1\Sigma_g^+) + CH_3CCH$  reaction. Also, our treatment cannot account for impact-parameter dependent reaction dynamics. Therefore, the calculated product branching ratios calculated here might differ from those derived in actual crossed beam experiments. The overall kinetic scheme used in our calculations is shown in Figure 8. We included into our consideration all reaction channels, i.e., H and  $H_2$  eliminations as well as various

**TABLE 1: Rate Constants ( $s^{-1}$ ) for Individual Reaction Steps Calculated Using RRKM and Microcanonical VTS Theories for Collision Energies in the Range of 0–50 kJ/mol (0–11.95 kcal/mol)**

| reaction  | $\sigma^a$ | collision energy, kJ/mol (kcal/mol) |                       |                       |                       |                       |
|---|------------|-------------------------------------|-----------------------|-----------------------|-----------------------|-----------------------|
|   |            | 0 (0)                               | 10 (2.39)             | 20 (4.78)             | 30 (7.17)             | 40 (9.56)             |
| 1 → 2   | 1          | $1.62 \times 10^{11}$               | $1.77 \times 10^{11}$ | $1.92 \times 10^{11}$ | $2.08 \times 10^{11}$ | $2.25 \times 10^{11}$ |
| 2 → 1   | 1          | $6.51 \times 10^{11}$               | $7.11 \times 10^{11}$ | $7.74 \times 10^{11}$ | $8.38 \times 10^{11}$ | $9.04 \times 10^{11}$ |
| 2 → 3   | 1          | $4.12 \times 10^{11}$               | $4.76 \times 10^{11}$ | $5.41 \times 10^{11}$ | $6.13 \times 10^{11}$ | $6.9 \times 10^{11}$  |
| 3 → 2   | 1          | $6.31 \times 10^6$                  | $8.7 \times 10^6$     | $1.18 \times 10^7$    | $1.58 \times 10^7$    | $2.1 \times 10^7$     |
| 3 → 4   | 3          | $1.19 \times 10^9$                  | $1.51 \times 10^9$    | $1.89 \times 10^9$    | $2.34 \times 10^9$    | $2.87 \times 10^9$    |
| 4 → 3   | 1          | $3.45 \times 10^{11}$               | $3.82 \times 10^{11}$ | $4.23 \times 10^{11}$ | $4.65 \times 10^{11}$ | $5.1 \times 10^{11}$  |
| 3 → HCCCCCH + H <sub>2</sub>  | 3          | $4.73 \times 10^6$                  | $7.67 \times 10^6$    | $1.21 \times 10^7$    | $1.86 \times 10^7$    | $2.8 \times 10^7$     |
| 4 → 5   | 1          | $5.36 \times 10^{11}$               | $5.69 \times 10^{11}$ | $6.03 \times 10^{11}$ | $6.37 \times 10^{11}$ | $6.71 \times 10^{11}$ |
| 5 → 4   | 1          | $6.18 \times 10^9$                  | $7.4 \times 10^9$     | $8.81 \times 10^9$    | $1.04 \times 10^{10}$ | $1.22 \times 10^{10}$ |
| 4 → 8   | 1          | $1.97 \times 10^{12}$               | $1.99 \times 10^{12}$ | $2.01 \times 10^{12}$ | $2.03 \times 10^{12}$ | $2.05 \times 10^{12}$ |
| 8 → 4   | 1          | $5.49 \times 10^{11}$               | $6.03 \times 10^{11}$ | $6.59 \times 10^{11}$ | $7.18 \times 10^{11}$ | $7.8 \times 10^{11}$  |
| 4 → H <sub>2</sub> CCCCCH + H   | 1          | $9.18 \times 10^9$                  | $1.22 \times 10^{10}$ | $1.59 \times 10^{10}$ | $2.04 \times 10^{10}$ | $2.58 \times 10^{10}$ |
| 5 → 6   | 2          | $1.52 \times 10^9$                  | $1.85 \times 10^9$    | $2.23 \times 10^9$    | $2.68 \times 10^9$    | $3.19 \times 10^9$    |
| 6 → 5   | 1          | $3.17 \times 10^{12}$               | $3.32 \times 10^{12}$ | $3.46 \times 10^{12}$ | $3.6 \times 10^{12}$  | $3.74 \times 10^{12}$ |
| 5 → 9   | 1          | $1.73 \times 10^9$                  | $2.19 \times 10^9$    | $2.76 \times 10^9$    | $3.42 \times 10^9$    | $4.22 \times 10^9$    |
| 9 → 5   | 1          | $8.14 \times 10^{10}$               | $9.8 \times 10^{10}$  | $1.17 \times 10^{11}$ | $1.39 \times 10^{11}$ | $1.63 \times 10^{11}$ |
| 5 → HCCCHCC + H <sub>2</sub>  | 1          | $1.17 \times 10^7$                  | $1.8 \times 10^7$     | $2.72 \times 10^7$    | $4.01 \times 10^7$    | $5.79 \times 10^7$    |
| 6 → 7   | 1          | $2.65 \times 10^{12}$               | $2.86 \times 10^{12}$ | $3.07 \times 10^{12}$ | $3.3 \times 10^{12}$  | $3.53 \times 10^{12}$ |
| 7 → 6   | 4          | $1.86 \times 10^9$                  | $2.32 \times 10^9$    | $2.87 \times 10^9$    | $3.51 \times 10^9$    | $4.27 \times 10^9$    |
| 6 → 10  | 1          | $4.84 \times 10^{12}$               | $4.84 \times 10^{12}$ | $4.85 \times 10^{12}$ | $4.86 \times 10^{12}$ | $4.86 \times 10^{12}$ |
| 10 → 6  | 2          | $7.07 \times 10^{10}$               | $7.91 \times 10^{10}$ | $8.82 \times 10^{10}$ | $9.79 \times 10^{10}$ | $1.08 \times 10^{11}$ |
| 6 → HCCCHCCCH + H   | 1          | $8.8 \times 10^{10}$                | $1.15 \times 10^{11}$ | $1.49 \times 10^{11}$ | $1.89 \times 10^{11}$ | $2.37 \times 10^{11}$ |
| 7 → HCCCCCH + H <sub>2</sub>  | 1          | $7.94 \times 10^6$                  | $1.28 \times 10^7$    | $2 \times 10^7$       | $3.05 \times 10^7$    | $4.56 \times 10^7$    |
| 8 → 10  | 2          | $1.46 \times 10^5$                  | $2.78 \times 10^5$    | $5.06 \times 10^5$    | $8.83 \times 10^5$    | $1.49 \times 10^6$    |
| 10 → 8  | 2          | $1.85 \times 10^5$                  | $3.51 \times 10^5$    | $6.35 \times 10^5$    | $1.1 \times 10^6$     | $1.85 \times 10^6$    |
| 8 → 13  | 1          | $5.75 \times 10^{10}$               | $6.51 \times 10^{10}$ | $7.34 \times 10^{10}$ | $8.23 \times 10^{10}$ | $9.19 \times 10^{10}$ |
| 13 → 8  | 3          | $3.45 \times 10^{11}$               | $3.61 \times 10^{11}$ | $3.77 \times 10^{11}$ | $3.93 \times 10^{11}$ | $4.08 \times 10^{11}$ |
| 8 → HC <sub>2</sub> -cyc-C <sub>3</sub> H + H <sub>2</sub>              | 1          | $2.35 \times 10^6$                  | $4.03 \times 10^6$    | $6.68 \times 10^6$    | $1.07 \times 10^7$    | $1.67 \times 10^7$    |
| 9 → 11  | 2          | $4.01 \times 10^8$                  | $5.26 \times 10^8$    | $6.8 \times 10^8$     | $8.68 \times 10^8$    | $1.1 \times 10^9$     |
| 11 → 9  | 2          | $6.87 \times 10^{10}$               | $7.87 \times 10^{10}$ | $8.95 \times 10^{10}$ | $1.01 \times 10^{11}$ | $1.13 \times 10^{11}$ |
| 9 → 14  | 2          | $2.07 \times 10^7$                  | $3.06 \times 10^7$    | $4.42 \times 10^7$    | $6.26 \times 10^7$    | $8.69 \times 10^7$    |
| 14 → 9  | 1          | $2.5 \times 10^{10}$                | $3.22 \times 10^{10}$ | $4.07 \times 10^{10}$ | $5.08 \times 10^{10}$ | $6.24 \times 10^{10}$ |
| 9 → C <sub>2</sub> = cyc-C <sub>3</sub> H <sub>2</sub> + H <sub>2</sub> | 1          | $4.27 \times 10^5$                  | $8.28 \times 10^5$    | $1.53 \times 10^6$    | $2.69 \times 10^6$    | $4.57 \times 10^6$    |
| 11 → 12   | 1          | $8.04 \times 10^{12}$               | $8.06 \times 10^{12}$ | $8.07 \times 10^{12}$ | $8.09 \times 10^{12}$ | $8.1 \times 10^{12}$  |
| 12 → 11   | 2          | $6.91 \times 10^8$                  | $8.32 \times 10^8$    | $9.9 \times 10^8$     | $1.18 \times 10^9$    | $1.3 \times 10^9$     |
| 12 → H <sub>2</sub> CCCCC + H <sub>2</sub>                              | 2          | $6.33 \times 10^6$                  | $9.89 \times 10^6$    | $1.51 \times 10^7$    | $2.25 \times 10^7$    | $3.28 \times 10^7$    |
| 13 → HC <sub>2</sub> -cyc-C <sub>3</sub> H + H <sub>2</sub>             | 3          | $3.98 \times 10^5$                  | $7.46 \times 10^5$    | $1.33 \times 10^6$    | $2.26 \times 10^6$    | $3.69 \times 10^6$    |
| 14 → c-C <sub>3</sub> H <sub>2</sub> + C <sub>2</sub> H <sub>2</sub>    | 1          | $5.24 \times 10^{12}$               | $5.96 \times 10^{12}$ | $6.73 \times 10^{12}$ | $7.53 \times 10^{12}$ | $8.38 \times 10^{12}$ |
| 1 → 15  | 1          | $3.79 \times 10^6$                  | $7.27 \times 10^6$    | $1.31 \times 10^7$    | $2.25 \times 10^7$    | $3.68 \times 10^7$    |
| 15 → 1  | 1          | $1.87 \times 10^9$                  | $2.99 \times 10^9$    | $4.54 \times 10^9$    | $6.61 \times 10^9$    | $9.29 \times 10^9$    |
| 15 → 16   | 1          | $2.86 \times 10^{12}$               | $2.9 \times 10^{12}$  | $2.95 \times 10^{12}$ | $2.99 \times 10^{12}$ | $3.03 \times 10^{12}$ |
| 16 → 15   | 1          | $1.41 \times 10^8$                  | $1.85 \times 10^8$    | $2.4 \times 10^8$     | $3.06 \times 10^8$    | $3.85 \times 10^8$    |
| 16 → H <sub>2</sub> CCCCC + H <sub>2</sub>                              | 3          | 0                                   | 0                     | 0                     | 0                     | 1.06                  |
| 3 → 16  | 1          | $1.04 \times 10^7$                  | $1.61 \times 10^7$    | $2.42 \times 10^7$    | $3.57 \times 10^7$    | $5.17 \times 10^7$    |
| 16 → 3  | 1          | $4.12 \times 10^9$                  | $5.71 \times 10^9$    | $7.75 \times 10^9$    | $1.03 \times 10^{10}$ | $1.36 \times 10^{10}$ |
| VTS1, 3 → H <sub>2</sub> CCCCCH + H                                     | 3          | $1.98 \times 10^8$                  | $2.79 \times 10^8$    | $3.86 \times 10^8$    | $5.26 \times 10^8$    | $7.07 \times 10^8$    |
| VTS2, 5 → H <sub>2</sub> CCCCCH + H                                     | 1          | $2.12 \times 10^8$                  | $3.01 \times 10^8$    | $4.1 \times 10^8$     | $5.5 \times 10^8$     | $7.28 \times 10^8$    |
| VTS3, 5 → HCCCHCCCH + H   | 2          | $2.65 \times 10^8$                  | $3.68 \times 10^8$    | $5.04 \times 10^8$    | $6.81 \times 10^8$    | $9.07 \times 10^8$    |
| VTS4, 7 → HCCCHCCCH + H   | 2          | $1.09 \times 10^8$                  | $1.58 \times 10^8$    | $2.23 \times 10^8$    | $3.11 \times 10^8$    | $4.25 \times 10^8$    |
| VTS5, 12 → H <sub>2</sub> CCCCCH + H                                    | 4          | $3.52 \times 10^8$                  | $4.93 \times 10^8$    | $6.8 \times 10^8$     | $9.1 \times 10^8$     | $1.2 \times 10^9$     |
| VTS6, 7 → C <sub>3</sub> H <sub>3</sub> + C <sub>2</sub> H              | 2          | $7.6 \times 10^5$                   | $1.88 \times 10^6$    | $4.19 \times 10^6$    | $8.72 \times 10^6$    | $1.7 \times 10^7$     |
| VTS7, 3 → CH <sub>3</sub> + C <sub>4</sub> H                            | 1          | $2.12 \times 10^3$                  | $5.39 \times 10^3$    | $1.26 \times 10^4$    | $2.73 \times 10^4$    | $5.56 \times 10^4$    |
| VTS8, 4 → C <sub>2</sub> H <sub>3</sub> + C <sub>3</sub> H              | 1          | 0                                   | 0                     | 2.19                  | $4.54 \times 10^2$    | $5.74 \times 10^3$    |
| VTS9, 5 → C <sub>3</sub> H <sub>3</sub> + C <sub>2</sub> H              | 1          | $3.95 \times 10^6$                  | $8.1 \times 10^6$     | $1.52 \times 10^7$    | $2.75 \times 10^7$    | $4.77 \times 10^7$    |
| VTS10, 16 → C <sub>4</sub> + CH <sub>4</sub>                            | 1          | 0                                   | 8.58                  | $6.98 \times 10^2$    | $6.89 \times 10^3$    | $3.29 \times 10^4$    |

<sup>a</sup> Reaction path degeneracy.

heavy-fragment formation channels. For the H loss, single C–C bond cleavage, and CH<sub>4</sub> loss pathways, which do not have exit barriers, we applied microcanonical variational transition state theory (VTST). The reaction coordinates in our calculations were chosen as the lengths of breaking C–H and C–C bonds, or, in the case of the **16** → C<sub>4</sub> + CH<sub>4</sub> reaction, as the distance between the terminal carbon atom of C<sub>4</sub> and the center of the C–H bond in the methane fragment. Totally, as shown in Figure 8, 10 different variational transition states, VTS1–VTS10, and corresponding rate constants were determined.

In the kinetic scheme, we assumed that the reaction starts from the energized (chemically activated) intermediates **1** and

**2**. The internal energy available to these intermediates equals to the energy of chemical activation, i.e., the well depth at these local minima with respect to the C<sub>2</sub>(<sup>1</sup>S<sub>g</sub><sup>+</sup>) + CH<sub>3</sub>CCH reactants plus collision energy,  $E_{\text{col}}$ , assuming that the dominant fraction of the latter is converted to the vibrational energy of the intermediates and only a small fraction goes to their rotational excitation. Rate constants were calculated for different collision energies, from 0 to 50 kJ/mol (0–11.95 kcal/mol), to match the conditions of future crossed molecular beam experiment to be performed for this reaction. The calculated values of rate constants are collected in Table 1. As one can see, all rate constants at these conditions are safely lower than 10<sup>13</sup> s<sup>-1</sup>, the

**TABLE 2: Branching Ratios (%) of Various Products of the  $C_2(X^1\Sigma_g^+)$  +  $CH_3CCH(X^1A_1)$  Reaction**

| products               | collision energy, kJ/mol (kcal/mol) |                      |                      |                      |           |            |
|------------------------|-------------------------------------|----------------------|----------------------|----------------------|-----------|------------|
|                        | 0 (0)                               | 10 (2.39)            | 20 (4.78)            | 30 (7.17)            | 40 (9.56) | 50 (11.95) |
| $H_2CCCCCH + H$        | 64.1                                | 64.6                 | 65.0                 | 65.4                 | 65.9      | 66.2       |
| $HCCCHCCH + H$         | 33.8                                | 33.0                 | 32.2                 | 31.4                 | 30.5      | 29.7       |
| $HCCCCCH + H_2$        | 1.2                                 | 1.4                  | 1.6                  | 1.9                  | 2.1       | 2.4        |
| $HCCCHCC + H_2$        | 0.6                                 | 0.6                  | 0.7                  | 0.7                  | 0.7       | 0.8        |
| $C_2=cyc-C_3H_2 + H_2$ | $4.5 \times 10^{-4}$                | $6.3 \times 10^{-4}$ | $8.7 \times 10^{-4}$ | 0.0                  | 0.0       | 0.0        |
| $HC_2=cyc-C_3H + H_2$  | 0.0                                 | 0.0                  | 0.0                  | 0.0                  | 0.0       | 0.0        |
| $H_2CCCC + H_2$        | 0.0                                 | 0.0                  | 0.0                  | 0.0                  | 0.0       | 0.0        |
| $C_3H_3 + C_2H$        | 0.2                                 | 0.3                  | 0.4                  | 0.6                  | 0.7       | 0.9        |
| $c-C_3H_2 + C_2H_2$    | 0.0                                 | 0.0                  | 0.0                  | 0.1                  | 0.1       | 0.1        |
| $CH_3 + C_4H$          | $1.7 \times 10^{-4}$                | $3 \times 10^{-4}$   | $5.2 \times 10^{-4}$ | $8.3 \times 10^{-4}$ | 0.0       | 0.0        |
| $C_2H_3 + C_3H$        | 0                                   | 0.0                  | 0.0                  | 0.0                  | 0.0       | 0.0        |
| $C_4 + CH_4$           | 0                                   | 0.0                  | 0.0                  | 0.0                  | 0.0       | 0.0        |

applicability limit of RRKM theory corresponding to a typical rate of intramolecular vibrational redistribution (IVR). This indicates that, most likely, isomerization and decomposition of the energized  $C_5H_4$  intermediates formed in the  $C_2(X^1\Sigma_g^+)$  +  $CH_3CCH$  reaction should exhibit a statistical (RRKM) behavior, although a comparison of the present theoretical result with future experimental data will actually address this issue.

Since both intermediates **1** and **2** can be formed directly from the reactants without a barrier, in the calculations of product branching ratios we considered different relative initial concentrations of **1** and **2**, from 100/0 to 0/100. However, the resulting branching ratios appeared to be insensitive to this parameter, because both **1** and **2** nearly exclusively isomerize to intermediate **3**. The only other possible channel is the rearrangement of **1** to **15** and then to **16**, and so forth; however, the rate constants for the **1** → **15** reaction are about 4 orders of magnitude lower than those for **1** → **2** and **2** → **3**, so that the reaction pathway via **15** is not competitive.

The calculated product branching ratios for  $E_{col} = 0$ –11.95 kcal/mol are shown in Table 2. One can see that the dominant reaction products are  $C_5H_3$  radicals + H; the branching ratios of the  $H_2CCCCCH$  and  $HCCCHCCH$  isomers vary in the ranges 64–66% and 34–30%, respectively. Most of the  $H_2CCCCCH$  radicals, about 72% of their total amount, are produced by H elimination directly from methylacetylene **3** and the rest are formed from **4** and **5**, about 10% and 18%, respectively. The  $HCCCHCCH$  radicals mostly result from the H loss from **5** (71.7%) and to a less extent from dissociation of **6** (10.6%) and **7** (17.7%). Interestingly, significant fractions of both  $C_5H_3$  isomers are predicted to be produced from **4** and **6**, for which the H loss exhibits distinct exit barriers. This fact should be reflected in a shift of the maximum in the product translational energy distributions away from zero and can be tested in future crossed molecular beam experiments. The higher yield of the  $H_2CCCCCH$  isomer as compared to  $HCCCHCCH$  cannot be attributed to the small energetic preference (only 0.3 kcal/mol) of the former. Actually, the rate constants  $k(VTS3)$  for the formation of  $HCCCHCCH$  from **5** are slightly higher than  $k(VTS2)$  for the formation of  $H_2CCCCCH$  from the same precursor. The major reason for the higher branching ratio of  $H_2CCCCCH$  is that intermediate **5** yields both  $H_2CCCCCH$  and  $HCCCHCCH$ , while **3** yields solely the former, all three dissociation steps having roughly equal rates, for instance, about  $3 \times 10^8$  s<sup>-1</sup> at  $E_{col} = 10$  kJ/mol (Table 1).

The most important minor products of the  $C_2(X^1\Sigma_g^+)$  +  $CH_3CCH$  reaction are  $HCCCCCH + H_2$  (up to 2.4% at the highest collision energy) and  $HCCCHCC + H_2$  (up to 0.8%). The former product pair is mostly produced from intermediate

**3**, and the latter from **5**. Again, as in the case of H loss, the barriers for  $H_2$  elimination leading to the two products are not very different, and the corresponding rate constants the final reaction step are even higher for the case of  $HCCCHCC$  than for  $HCCCCCH$ . However, the fact that H<sub>2</sub> elimination from **5** faces relatively more competition from fragmentation to H +  $C_5H_3$  (through two different routes) than is the case for **3** leads to a smaller branching ratio of  $HCCCHCC$ . Among the heavy-fragment products, we expect that only  $C_3H_3 + C_2H$  (up to 0.9%) and  $c-C_3H_2 + C_2H_2$  (up to 0.1%) might be detected experimentally at high collision energies. Although the energetics is more favorable for  $c-C_3H_2 + C_2H_2$  than for  $C_3H_3 + C_2H$ , the former product couple can be formed from **5** and **7** via loose transition states VTS9 and VTS6. Alternatively, the pathways leading to  $c-C_3H_2 + C_2H_2$  are significantly longer, via **4**, **8** (or **5** and **6**), **10**, and **14**, or **5**, **9**, and **14**, and they involve tight transition states for all reaction steps. This makes  $c-C_3H_2 + C_2H_2$  much less probable products than  $C_3H_3 + C_2H$ . The dependence of the branching ratios on the collision energy in the range  $E_{col} = 0$ –11.95 kcal/mol is found to be relatively minor; the yield of  $HCCCHCCH$  decreases from 33.8% to 29.7%, while the yields of the other significant products,  $H_2CCCCCH + H$ ,  $C_5H_2 + H_2$ ,  $C_3H_3 + C_2H$ , and  $c-C_3H_2 + C_2H_2$ , slightly increase.

#### 4. Conclusions

High-level ab initio calculations of PES of the  $C_2(X^1\Sigma_g^+)$  +  $CH_3CCH(X^1A_1)$  reaction demonstrate that the dicarbon molecule can add without an entrance barrier to the triple carbon–carbon bond of methylacetylene in the end-to-side and side-to-side manner to produce the three-member and four-member cyclic isomers **1** and **2** of the  $C_5H_4$  species. The intermediates **1** and **2** can rapidly rearrange to the most stable  $C_5H_4$  isomer **3**, methylacetylene, residing 137.6 kcal/mol below the initial reactants. The chemically activated structure **3** can decompose by losing a hydrogen atom from the methyl group to produce the  $H_2CCCCCH$  ( $C_{2v}$ ,  $^2B_1$ ) isomer of the  $C_5H_3$  radical or by splitting molecular hydrogen to yield  $HCCCCCH$  ( $C_{2v}$ ,  $^1A_1$ ). The  $H_2CCCCCH + H$  and  $HCCCCCH$  products are computed to be 46.0 and 50.0 kcal/mol exothermic. Alternatively, the methylacetylene intermediate can undergo a series of rearrangements by hydrogen migrations and ring-closure/ring-opening processes involving various chain and three-member ring local minima on the  $C_5H_4$  PES through transition states lying much lower in energy than the initial reactants. Dissociation of various intermediates can, in principle, produce a variety of different reaction products including  $C_5H_3$  ( $H_2CCCCCH$  or  $HCCCHCCH$ ) + H,  $C_5H_2$  ( $HCCCCCH$ ,  $HCCCHCC$ ,  $H_2CCCCC$ ,  $HC_2=cyc-C_3H$ , or  $C_2=cyc-C_3H_2$ ) +  $H_2$ , and heavy-fragment pairs

$\text{C}_3\text{H}_3 + \text{C}_2\text{H}$ ,  $c\text{-C}_3\text{H}_2 + \text{C}_2\text{H}_2$ ,  $\text{CH}_3 + \text{C}_4\text{H}$ ,  $\text{C}_4 + \text{CH}_4$ , and  $\text{C}_2\text{H}_3 + \text{C}_3\text{H}$ . All the products listed above lie lower in energy than  $\text{C}_2(^1\Sigma_g^+) + \text{CH}_3\text{CCH}(^1\text{A}_1)$ , except  $\text{C}_4(^1\Sigma_g^+) + \text{CH}_4$  and  $\text{C}_2\text{H}_3 + \text{C}_3\text{H}$ , which, respectively, are 2.8 and 4.2 kcal/mol endothermic.

Despite the fact that numerous products are energetically accessible, RRKM calculations of individual reaction rate constants and products branching show that, if the system behaves statistically, the dominant reaction products, 96–98% of the total product yield, should be  $\text{C}_5\text{H}_3 + \text{H}$ . The branching ratios of the  $\text{H}_2\text{CCCCCH}(\text{C}_{2v}, ^2\text{B}_1)$  and  $\text{HCCCHCCH}(\text{C}_{2v}, ^2\text{B}_1)$  isomers of  $\text{C}_5\text{H}_3$  are calculated as 64–66% and 34–30% at collision energies varying in the 0–11.95 kcal/mol range.  $\text{H}_2\text{CCCCCH}$  is mostly produced from the methyldiacetylene intermediate **3**, while  $\text{HCCCHCCH}$  is predominantly formed by the loss H from the intermediate **5**,  $\text{H}_2\text{CCCHCCH}$ , which in turn is produced from **3** by two sequential hydrogen shifts. The most significant minor reaction products are isomers of  $\text{C}_5\text{H}_2$  formed by elimination of molecular hydrogen from **3** ( $\text{HCCCCCH}$ , 1.2–2.4%) and from **5** ( $\text{HCCCHCC}$ , 0.6–0.8%). Among the heavy-fragment product pairs, we expect that only  $\text{C}_3\text{H}_3 + \text{C}_2\text{H}$  (0.2–0.9%) and  $c\text{-C}_3\text{H}_2 + \text{C}_2\text{H}_2$  (up to 0.1%) could be detected.

These investigations hold also strong implications for astrochemistry and for combustion flames. The barrierless reaction of dicarbon with methylacetylene underlines the potential contribution of this bimolecular reaction in cold molecular clouds such as the Taurus Molecular Cloud (TMC-1), W3(OH), W518, and Orion A.<sup>50</sup> Since deuterated methylacetylenes ( $\text{CH}_3\text{CCD}$ , and  $\text{CH}_2\text{DCCH}$ ) were identified in OMC-1 and TMC-1, formation of partially deuterated  $\text{C}_5\text{H}_2\text{D}$  is also expected to take place as well.<sup>51</sup> In summary, the ab initio/RRKM calculations clearly demonstrate that the barrierless  $\text{C}_2(^1\Sigma_g^+) + \text{CH}_3\text{CCH}(^1\text{A}_1)$  reaction under single-collision conditions should be a major source of  $\text{C}_5\text{H}_3$  radicals with the relative branching ratio of the  $\text{H}_2\text{CCCCCH}$  and  $\text{HCCCHCCH}$  isomers close to 2:1.

**Acknowledgment.** This work was funded by the Chemical Sciences, Geosciences and Biosciences Division, Office of Basic Energy Sciences, Office of Sciences of the U.S. Department of Energy (Grant DE-FG02-04ER15570 to FIU and Grant DE-FG02-03ER15411 to the University of Hawaii).

**Supporting Information Available:** Calculated total energies, ZPE, optimized Cartesian coordinates, and vibrational frequencies of all intermediates and transition states involved in the  $\text{C}_2(^1\Sigma_g^+) + \text{CH}_3\text{CCH}(^1\text{A}_1)$  reaction and full details of IRC calculations for TS2–3. This material is available free of charge via the Internet at <http://pubs.acs.org>.

## References and Notes

- (1) Baranovski, A. P.; McDonalds, J. R. *J. Phys. Chem.* **1977**, *66*, 3300.
- (2) Smith, G. P.; Park, C.; Schneiderman, J.; Luque, J. *Combust. Flame* **2005**, *141*, 66.
- (3) Weltner, W.; van Zee, R. *J. Chem. Rev.* **1989**, *89*, 1713.
- (4) John, P.; Rabeau, J. R.; Wilson, J. I. B. *Diamond Relat. Mater.* **2002**, *11*, 608.
- (5) (a) Gordon, A. G. *The Spectroscopy of Flames*; Wiley: New York, 1974. (b) Clary, D. C. *Annu. Rev. Phys. Chem.* **1990**, *41*, 61.
- (6) Yorka, S. B. *Astrophys. J.* **1983**, *88*, 1816.
- (7) Combi, M. R.; Fink, U. *Astrophys. J.* **1997**, *484*, 879.
- (8) Swamy, K. S. K. *Astrophys. J.* **1997**, *481*, 1004.
- (9) Rousselot, P.; Laffont, C.; Moreels G.; Clairemidi, J. *Astron. Astrophys.* **1998**, *335*, 765.
- (10) Shiomi, T.; Nagai, H.; Hiramatsu, M.; Nawata, M. *Diamond Relat. Mater.* **2001**, *10*, 388.
- (11) Goyette, A. N.; Matsuda, Y.; Anderson, L. W.; Lawler, J. E. *J. Vac. Sci. Technol., A* **1998**, *16*, 337.
- (12) Hiramatsu, M.; Kato, K.; Lau C. H.; Ford, J. S.; Hori, M. *Diamond Relat. Mater.* **2003**, *12*, 365.
- (13) Pascoli, G.; Polleux, A. *Astron. Astrophys.* **2000**, *359*, 799.
- (14) Hill, H. G. M.; Jones, A. P.; d'Hendecourt, L. B. *Astron. Astrophys.* **1998**, *336*, L41.
- (15) Andersen, A. C.; Jorgensen, U. G.; Nicolaisen, F. M.; Sorensen, P. G.; Glejbol, K. *Astron. Astrophys.* **1998**, *330*, 1080.
- (16) Rennick, C. J.; Smith, J. A.; Ashfold, M. N. R.; Orr-Ewing, A. J. *Chem. Phys. Lett.* **2004**, *383*, 518.
- (17) Winicur, D. H.; Hardwick, J. L.; Murphy, S. N. *Combust. Flame* **1983**, *53*, 93.
- (18) Chan, M. C.; Yeung, S.-H.; Wong, Y.-Y.; Li, Y.; Chan, W.-M.; Yim, K.-H. *Chem. Phys. Lett.* **2004**, *390*, 340.
- (19) Necula, A.; Scott, L. T. *J. Am. Chem. Soc.* **2000**, *122*, 1548.
- (20) Taylor, R.; Langley, G. J.; Kroto, H. W.; Walton, D. R. M. *Nature* **1993**, *366*, 728.
- (21) Battin-Leclerc, F. *Phys. Chem. Chem. Phys.* **2002**, *4*, 2072.
- (22) Richter, H.; Howard, J. B. *Phys. Chem. Chem. Phys.* **2002**, *4*, 2038.
- (23) Kaiser, R. I.; Mebel, A. M. *Int. Rev. Phys. Chem.* **2002**, *21*, 307 and references therein.
- (24) Frenklach, M. *Phys. Chem. Chem. Phys.* **2002**, *4*, 2028.
- (25) Miller, J. A. *Faraday Discuss.* **2001**, *119*, 461.
- (26) Huang, C.; Hu, Z.; Xin, Y.; Pei, L.; Chen, Y. *J. Chem. Phys.* **2004**, *120*, 2225.
- (27) Wang, H.; Zhu, Z.; Zhang, S.; Pei, L.; Chen, Y. *Chem. Phys. Lett.* **2005**, *407*, 217.
- (28) Martin, M. *J. Photochem. Photobiol., A* **1992**, *66*, 263.
- (29) Huang, C.; Zhu, Z.; Wang, H.; Pei, L.; Chen, Y. *J. Phys. Chem. A* **2005**, *109*, 3921.
- (30) Savic, I.; Cermak, I.; Gerlich, D. *Int. J. Mass Spectrom.* **2005**, *240*, 139.
- (31) Balucani, N.; Mebel, A. M.; Lee, Y. T.; Kaiser, R. I. *J. Phys. Chem. A* **2001**, *105*, 9813.
- (32) Kaiser, R. I.; Le, T. N.; Nguyen, T. L.; Mebel, A. M.; Balucani, N.; Lee, Y. T.; Stahl, F.; Schleyer, P. v. R.; Schaefer, H. F., III. *Faraday Discuss.* **2001**, *119*, 51.
- (33) Kaiser, R. I.; Balucani, N.; Charkin, D. O.; Mebel, A. M. *Chem. Phys. Lett.* **2003**, *382*, 112.
- (34) Gu, X.; Guo, Y.; Mebel, A. M.; Kaiser, R. I. *Phys. Chem. Chem. Phys.*, submitted.
- (35) Mebel, A. M.; Lin, S. H.; Yang, X. M.; Lee, Y. T. *J. Phys. Chem. A* **1997**, *101*, 6781.
- (36) Kislov, V. V.; Nguyen, T. L.; Mebel, A. M.; Lin, S. H.; Smith, S. *C. J. Chem. Phys.* **2004**, *120*, 7008.
- (37) Becke, A. D. *J. Chem. Phys.* **1993**, *98*, 5648.
- (38) Lee, C.; Yang, W.; Parr, R. G. *Phys. Rev. B* **1988**, *37*, 785.
- (39) Mebel, A. M.; Morokuma, K.; Lin, M. C. *J. Chem. Phys.* **1995**, *103*, 7414.
- (40) (a) Purvis, G. D.; Bartlett, R. J. *J. Chem. Phys.* **1982**, *76*, 1910. (b) Scuseria, G. E.; Janssen, C. L.; Schaefer, H. F., III. *J. Chem. Phys.* **1988**, *89*, 7382. (c) Scuseria, G. E.; Schaefer, H. F., III. *J. Chem. Phys.* **1989**, *90*, 3700; Pople, J. A.; Head-Gordon, M.; Raghavachari, K. *J. Chem. Phys.* **1987**, *87*, 5968.
- (41) (a) Werner, H.-J.; Knowles, P. J. *J. Chem. Phys.* **1985**, *82*, 5053. (b) Knowles, P. J.; Werner, H.-J. *Chem. Phys. Lett.* **1985**, *115*, 259.
- (42) (a) Werner, H.-J.; Knowles, P. J. *J. Chem. Phys.* **1988**, *89*, 5803. (b) Knowles, P. J.; Werner, H.-J. *Chem. Phys. Lett.* **1988**, *145*, 514.
- (43) Frisch, M. J.; Trucks, G. W.; Schlegel, H. B.; Scuseria, G. E.; Robb, M. A.; Cheeseman, J. R.; Zakrzewski, V. G.; Montgomery, J. A., Jr.; Stratmann, R. E.; Burant, J. C.; Dapprich, S.; Millam, J. M.; Daniels, A. D.; Kudin, K. N.; Strain, M. C.; Farkas, O.; Tomasi, J.; Barone, V.; Cossi, M.; Cammi, R.; Mennucci, B.; Pomelli, C.; Adamo, C.; Clifford, S.; Ochterski, J.; Petersson, G. A.; Ayala, P. Y.; Cui, Q.; Morokuma, K.; Malick, D. K.; Rabuck, A. D.; Raghavachari, K.; Foresman, J. B.; Cioslowski, J.; Ortiz, J. V.; Baboul, A. G.; Stefanov, B. B.; Liu, G.; Liashenko, A.; Piskorz, P.; Komaromi, I.; Gomperts, R.; Martin, R. L.; Fox, D. J.; Keith, T.; Al-Laham, M. A.; Peng, C. Y.; Nanayakkara, A.; Gonzalez, C.; Challacombe, M.; Gill, P. M. W.; Johnson, B.; Chen, W.; Wong, M. W.; Andres, J. L.; Head-Gordon, M.; Replogle, E. S.; Pople, J. A. *Gaussian 98*, revision A.9; Gaussian, Inc.: Pittsburgh, PA, 1998.
- (44) Amos, R. D.; Bernhardsson, A.; Berning, A.; Celani, P.; Cooper, D. L.; Deegan, M. J. O.; Dobbyn, A. J.; Eckert, F.; Hampel, C.; Hetzer, G.; Knowles, P. J.; Korona, T.; Lindh, R.; Lloyd, A. W.; McNicholas, S. J.; Manby, F. R.; Meyer, W.; Mura, M. E.; Nicklass, A.; Palmieri, P.; Pitzer,

- R.; Rauhut, G.; Schütz, M.; Schumann, U.; Stoll, H.; Stone, A. J.; Tarroni, R.; Thorsteinsson, T.; Werner, H.-J. *MOLPRO*, version 2002.6; University of Birmingham: Birmingham, U.K., 2003.
- (45) Eyring, H.; Lin, S. H.; Lin, S. M. *Basic Chemical Kinetics*; Wiley: New York, 1980.
- (46) Robinson, P. J.; Holbrook, K. A. *Unimolecular Reactions*; Wiley: New York, 1972.
- (47) Steinfield, J. I.; Francisco, J. S.; Hase, W. L. *Chemical Kinetics and Dynamics*; Prentice Hall: Englewood Cliffs, NJ, 1999.

- (48) Gonzales, C.; Schlegel, H. B. *J. Chem. Phys.* **1989**, *90*, 2154.
- (49) (a) Nguyen, T. L.; Mebel, A. M.; Kaiser, R. I. *J. Phys. Chem. A* **2001**, *105*, 3284. (b) Nguyen, T. L.; Mebel, A. M.; Lin, S. H.; Kaiser, R. I. *J. Phys. Chem. A* **2001**, *105*, 11549.
- (50) (a) Askne, J.; Hoeglund, B.; Hjalmarson, A.; Irvine, W. M *Astron. Astrophys.* **1984**, *130*, 311. (b) Gerin, M.; Combes, F.; Wlodarczak, G.; Encrénaz, P.; Laurent, C. *Astron. Astrophys.* **1992**, *253*, L29.
- (51) Irvine, W. M.; Hoglund, B.; Friberg, P.; Askne, J.; Ellder, J. *Astrophys. J.* **1981**, *248*, L113.